REVIEW ARTICLE | MARCH 25 2026

Liquid crystal enabled nonlinear optics and quantum optics

Special Collection: Quantum Light

Li-Lan Tian ; Fan Zou ; Jin-Tao Pan ; Ze-Nian Wu ; Yang Wei ; Yi-Hao Wei ; Ling-Ling Ma ; Yan-Qing Lu

Appl. Phys. Rev. 13, 011328 (2026)
https://doi.org/10.1063/5.0273606

Applied Physics Reviews REVIEW pubs.aip.org/aip/are

Liquid crystal enabled nonlinear optics and quantum optics

Cite as: Appl. Phys. Rev. **13**, 011328 (2026); doi: 10.1063/5.0273606
Submitted: 5 September 2025 · Accepted: 2 March 2026 ·
Published Online: 25 March 2026

Li-Lan Tian,[1] Fan Zou,[1] Jin-Tao Pan,[2] Ze-Nian Wu,[1] Yang Wei,[2] Yi-Hao Wei,[2] Ling-Ling Ma,[2,a)] and Yan-Qing Lu[2,a)]

AFFILIATIONS

[1]School of Physics, Chengdu University of Technology, Chengdu 610059, China
[2]National Laboratory of Solid State Microstructures, Key Laboratory of Intelligent Optical Sensing and Manipulation, College of Engineering and Applied Sciences, Collaborative Innovation Center of Advanced Microstructures, Nanjing University, Nanjing 210023, China

Note: This paper is part of the Special Topic, Quantum Light.
[a)]**Authors to whom correspondence should be addressed:** malingling@nju.edu.cn and yqlu@nju.edu.cn

ABSTRACT

Liquid crystals (LCs), due to their intrinsic optical anisotropy and strong response to external stimuli, have emerged as a critical bridge between classical optics and quantum photonics. Initially recognized for their transformative impact on display technologies, LCs have garnered increasing attention in recent years within the fields of nonlinear optics (NLO) and quantum optics, driven by their advantages such as electrically tunable birefringence, reconfigurable molecular alignment, and compatibility with compact photonic architectures. This review provides a comprehensive overview of the latest advancements in LC-enabled linear, nonlinear, and quantum optical systems. We begin by discussing the fundamental optical properties and phase states of LCs. Building upon this, we focus on the emerging field of ferroelectric nematic LCs (FNLCs), which, owing to their spontaneous polarization and unique molecular alignment control, demonstrate significantly enhanced second-order nonlinear effects. Helical derivatives of FNLCs further enhance polarization control, giving rise to new concepts in nonlinear geometric phase. Additionally, this paper highlights the applications of FNLCs in quantum photonics, including entangled photon generation and polarization state manipulation. These innovations overcome the limitations of time-reversal symmetry inherent in traditional systems, offering promising opportunities for unidirectional quantum communication, secure quantum networks, and high-fidelity quantum state manipulation. Finally, we discuss the challenges currently facing this field and explore future prospects for FNLCs in interdisciplinary domains such as linear photonics, NLO, and quantum engineering.

TABLE OF CONTENTS

I. INTRODUCTION

Over the past few decades, the development of photonic technologies[1–11] has been intricately intertwined with the discovery

and innovation of new optical materials.[12–16] Among these, liquid crystals (LCs) have emerged as a class of soft materials with high reconfigurability, standing out for their unique combination of fluidity and long-range molecular order,[17,18] thus exhibiting remarkable potential in optical control.[19,20] The inherent optical anisotropy of LC, along with their strong response to external stimuli—such as electric fields,[21,22] magnetic fields,[23,24] temperature changes,[25–27] mechanical stress, and light fields[28,29]—has made them indispensable functional media in various optical applications. These unique advantages have propelled LCs beyond their initial use in display technologies, positioning them as a highly versatile material platform in modern photonics. Whether at the macro or micro-nanoscale, LCs exhibit excellent programmability and compatibility, opening new pathways for the development of advanced optical systems.

Although LCs were initially applied mainly in display technologies, their use in advanced photonics has rapidly expanded. LCs are now widely used in dynamic optical modulation, wavefront shaping, and integrated nano-photonic platforms, and have formed key research directions in nonlinear optics (NLO)[36,39,40] and quantum optics[41,42] (as shown in Fig. 1).

Nonlinear optics focuses on the interaction between light and matter,[43–45] with fundamental processes such as second harmonic generation (SHG),[46] third harmonic generation (THG),[47] and spontaneous parametric downconversion (SPDC).[48–50] The realization of these processes often relies on materials with strong tunable light-matter coupling characteristics. Quantum optics, on the other hand, focuses on the quantum properties of light, with applications extending from entangled photon pair generation to the construction of reconfigurable quantum logic gates and quantum computing.[51–53] While the research focuses and technological paths of these two fields differ, they share stringent and highly overlapping requirements for active media—high response rates, wide tunability, and compatibility with miniaturized integrated architectures. These key characteristics are the core advantages inherently present in LCs. These core strengths of LCs offer a crucial direction to overcome the material bottleneck in nonlinear optics and quantum optics, and the discovery of ferroelectric nematic liquid crystals (FNLCs) has further elevated their application potential. In 2020, the team of Clark experimentally confirmed the existence of FNLCs for the first time,[32] a milestone achievement that not only filled a theoretical gap in the LC phase diagram but was also named one of

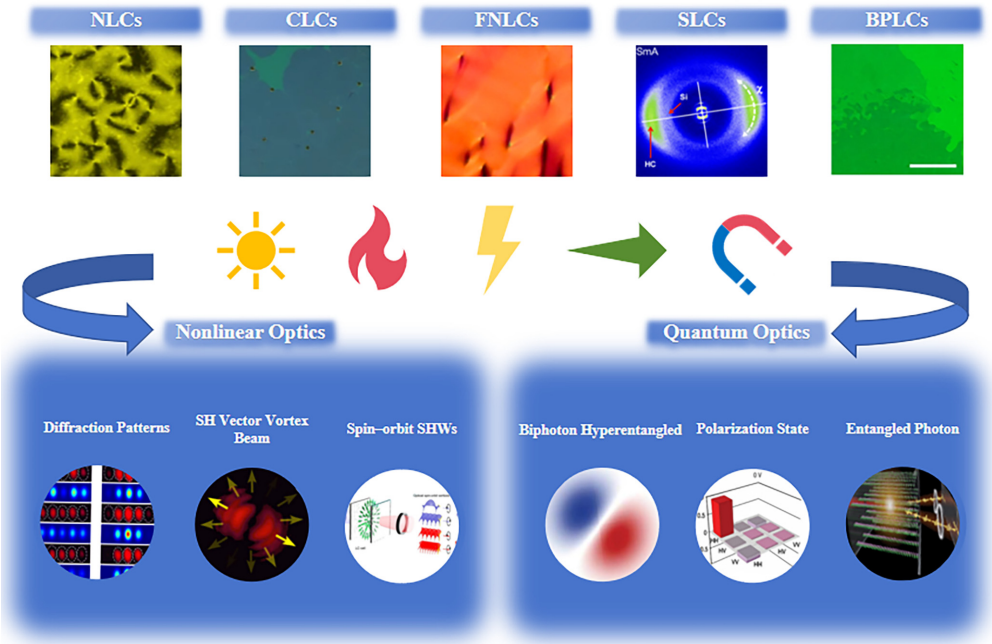

FIG. 1. Types of LCs: nematic liquid crystals(NLCs)[30] [Reproduced with permission from Ohzono *et al.*, Sci. Rep. **7**, 16814 (2017); Copyright 2017 Author(s), licensed under a Creative Commons Attribution (CC BY 4.0) license], cholesteric liquid crystals (CLCs)[31] [Reproduced with permission from Liu *et al.*, Nat. Commun. **13**, 2712 (2022); Copyright 2022 Author(s), licensed under a Creative Commons Attribution (CC BY 4.0) license], FNLCs[32] [Reproduced with permission from Chen *et al.*, Proc. Natl. Acad. Sci. U. S. A. **117**, 14021–14031 (2020); Copyright 2020 Author(s), licensed under a Creative Commons Attribution-NonCommercial-NoDerivatives (CC BY-NC-ND 4.0) license], smectic liquid crystals (SLCs)[33] [Reproduced with permission from Agra-Kooijman *et al.*, Phys. Rev. E **89**, 032506 (2014); Copyright 2014 American Physical Society], blue phase liquid crystals(BPLCs)[34] [Reproduced with permission from Lin *et al.*, Nat. Commun. **15**, 7038 (2024); Copyright 2024 Author(s), licensed under a Creative Commons Attribution (CC BY 4.0) license]. LC-enabled nonlinear and quantum optics: simulated and experimental diffraction patterns of second-harmonic signals[35] [Reproduced with permission from Chen *et al.*, Light: Sci. Appl. **14**, 314 (2025); Copyright 2025 Author(s), licensed under a Creative Commons Attribution (CC BY 4.0) license], SH vector vortex beam[36] [Reproduced with permission from Pan *et al.*, Nat. Commun. **15**, 8732 (2024); Copyright 2024 Author(s), licensed under a Creative Commons Attribution (CC BY 4.0) license], spin–orbit SHWs[36] [Reproduced with permission from Pan *et al.*, Nat. Commun. **15**, 8732 (2024); Copyright 2024 Author(s), licensed under a Creative Commons Attribution (CC BY 4.0) license], the biphoton hyperentangled state[37] [Reproduced with permission from Li *et al.*, Chin. Opt. Lett. **19**, 112601 (2021); Copyright 2021 Chinese Laser Press], polarization state[38] [Reproduced with permission from Sultanov *et al.*, Nature **631**, 8020 (2024); Copyright 2024 Author(s), licensed under a Creative Commons Attribution (CC BY 4.0) license], and entangled photon creation[38] [Reproduced with permission from Sultanov *et al.*, Nature **631**, 294–299 (2024); Copyright 2024 Author(s), licensed under a Creative Commons Attribution (CC BY 4.0) license].

"The Top Ten Breakthroughs of 2020" by *Physics World*. This achievement laid the experimental foundation for the application of FNLCs in both of these optical fields.

This review summarizes the latest research progress in LC-enabled photonics, covering linear optics, nonlinear optics, and quantum optics. It first provides an overview of the phase states of LC and their fundamental optical principles, laying the theoretical foundation for the subsequent discussions. The review further elaborates on the unique properties of FNLCs and their applications in nonlinear optics and quantum photonics. By tracing the development trajectory of the field—from fundamental physics research to device-level realization, from traditional technologies to emerging innovations—this paper outlines a clear development roadmap for LC photonics and offers a reference framework for future directions in this field.

II. LIQUID CRYSTALS

As a typical soft material, LCs combine both fluidity and long-range molecular order, a dual characteristic that grants them a rich array of optical properties, making them ideal candidates for advanced photonics applications. Structurally, LC molecules generally exhibit anisotropy (e.g., rod-like or disk-like morphology) and spontaneously align along a preferred direction, resulting in birefringence. This birefringence effect serves as the fundamental basis for the operation of most LC-based optical devices.[54]

A. Phase behavior

The discovery of LCs can be traced back to 1888, when Friedrich reported the unusual observation of compounds—cholesteryl benzoate and cholesteryl acetate—exhibiting two distinct melting points.[55] Subsequent polarized optical microscopy studies by Otto Lehmann revealed the presence of birefringence, a property characteristic of crystalline materials. In 1889, Lehmann coined the term "liquid crystal" to describe this intermediate state.[56] The LC phase represents a state of matter lying between crystalline solids and isotropic fluids.[56,57] Its phase behavior is not fixed but is dynamically governed by temperature, molecular structure, and external field conditions, enabling LCs to exhibit a wide range of phase transitions under varying environments. This tunability offers diverse opportunities for device applications. The emergence and stability of LC phases are inherently dependent on molecular shape and structure, which dictate the ordered arrangements in condensed LC states and, consequently, determine the type of LC phase exhibited.[58] Based on differences in the degree of positional and orientational order, LC phases can be classified into nematic, smectic, cholesteric, and other mesophases.

NLCs[59] represent the simplest structural form among anisotropic LC phases, exhibiting the lowest order parameter yet possessing the highest degree of symmetry. A schematic illustration of the molecular arrangement in this phase is shown in Fig. 2(a). In the nematic state, LC molecules display orientational order only along their long molecular axes, such that the long axes are, on average, aligned toward a common direction defined as the director (n). It should be noted that, on a statistical basis, the long axis of an individual molecule may deviate from n, yet the ensemble maintains macroscopic orientational uniformity. In contrast, NLCs lack significant positional ordering in molecular translation and do not form long-range crystalline lattices, thereby preserving fluidity and retaining liquid-like characteristics. Under crossed polarizers in a polarized optical microscope, NLCs with planar anchoring at the substrate typically exhibit characteristic schlieren textures, as illustrated in Fig. 2(b).

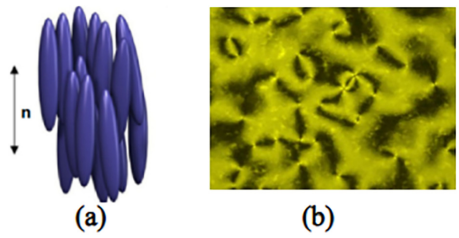

FIG. 2. (a) Molecular arrangement in the nematic phase of NLCs and (b) typical Schlieren texture of planar-anchored NLCs observed under a polarized light microscope.[30] Reproduced with permission from Ohzono *et al.*, Sci. Rep. **7**, 16814 (2017); Copyright 2017 Author(s), licensed under a Creative Commons Attribution (CC BY 4.0) license.

Smectic liquid crystal (SLCs)[60] typically emerge upon cooling from the nematic phase. In contrast to NLCs, which possess only orientational order, SLCs exhibit both orientational ordering and translational order of the molecular centers of mass, leading to the spontaneous formation of a layered structure. Within each layer, the molecular centers are distributed isotropically in the plane, with negligible positional correlation both within and between layers. As shown in Fig. 3, when the long molecular axes are aligned perpendicular to the layer plane, the phase is referred to as the smectic A (SmA) phase; if the long axes are tilted at a finite angle relative to the layer normal, the phase is classified as the smectic C (SmC) phase. The interlayer spacing in smectic phases is typically comparable to the molecular length, though it can be modulated by the molecular tilt angle. X ray diffraction (XRD) techniques are commonly employed to measure the layer spacing and determine the molecular orientation, thereby enabling reliable differentiation between SmA and SmC phases.[33]

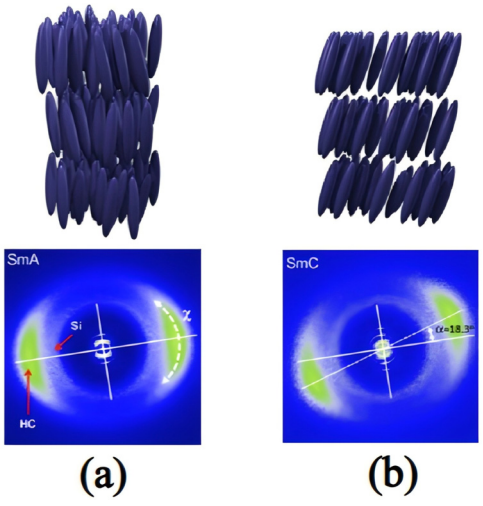

FIG. 3. Schematic representations of the molecular arrangements in the (a) SmA and (b) SmC phases, and the corresponding representative 2D-XRD patterns.[33] Reproduced with permission from Agra-Kooijman *et al.*, Phys. Rev. E **89**, 032506 (2014). Copyright 2014 American Physical Society.

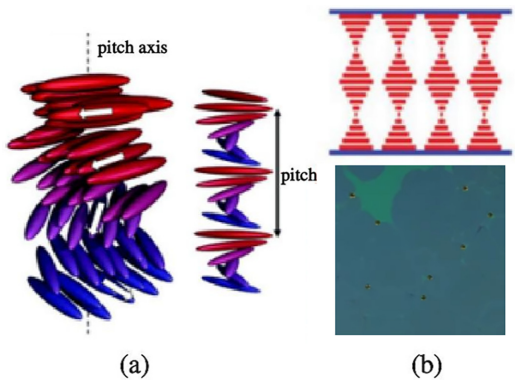

FIG. 4. (a) Molecular arrangement of CLCs. (b) Polarizing optical microscope (POM) textures of the helicoidal superstructure.[31] Reproduced with permission from Liu *et al.*, Nat. Commun. **13**, 2712 (2022). Copyright 2022 Author(s), licensed under a Creative Commons Attribution (CC BY 4.0) license.

From a thermodynamic perspective, cholesteric liquid crystals (CLCs)[61] can be regarded as the chiral variant of NLCs and are therefore also referred to as chiral nematic phases. A characteristic optical property of CLCs is *selective reflection*, which arises from their helical supramolecular structure. As shown in Fig. 4, the molecules are stacked with a fixed twist angle, forming a macroscopic helical structure characterized by the pitch (the distance required for the molecular orientation to complete a 360° rotation). When the incident light wavelength satisfies the Bragg matching condition, the light undergoes coherent superposition within the helical structure, resulting in a strong reflection band. This reflection exhibits intrinsic circular polarization selectivity: only light with the same handedness as the helix is reflected, while light with the opposite handedness is transmitted. A key advantage of this property is its wavelength tunability—external stimuli can reversibly modulate the pitch, thereby shifting the reflected wavelength. The reflectance is also angle-dependent. These features make CLCs highly promising for a wide range of photonic applications, including tunable filters, circular polarizers, reflective displays, and optical sensors.

B. Ferroelectric liquid crystals (FLCs)

To date, five categories of LCs with ferroelectric properties have been developed. The earliest discovery dates back to 1974, when a chiral ferroelectric smectic C was first reported.[62] This material exhibits exceptional characteristics, endowing it with promising potential for LC display technologies and nonlinear optical devices. Over the subsequent decades, researchers have developed a variety of new polar LC systems, including Chiral Columnar LCs,[63] Bent-core LCs,[64] Rigid linear polymer,[65,66] and Columnar FLCs.[67–69] These materials exhibit significant differences in molecular packing and local polarization orientation, with representative structures and polarization distributions shown in Fig. 5. The diversity in dielectric anisotropy, response mechanisms, and nonlinear optical properties across these configurations underpins the functional expansion of the ferroelectric LC family.

In conventional FLCs, the polarization mechanism primarily originates from the flexoelectric effect.[71] This effect typically relies on LCs with specific molecular geometries, such as pear-shaped molecules carrying a longitudinal dipole moment or banana-shaped molecules possessing a transverse dipole moment. Under an applied electric field, these molecular structures undergo controlled deformation, resulting in a macroscopic net polarization. However, in more symmetric rod-like LCs, even when dipole moments are present along the molecular long or short axes, their static arrangement or thermally driven dynamic motion often leads to mutual cancelation of dipole contributions. As a result, stable macroscopic polar domains are difficult to maintain.

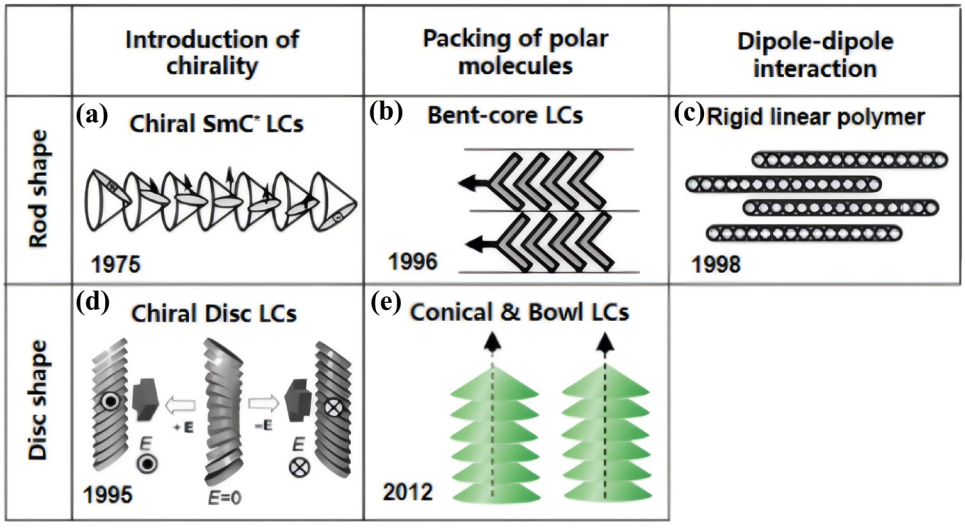

FIG. 5. Ferroelectric phases discovered prior to 2017: (a)–(e) correspond to chiral smectic phase LCs, polar chiral columnar LCs, bent-core polar LCs, rigid linear polymeric LCs, and columnar polar LCs.[70] Reproduced with permission from Takezoe *et al.*, Mol. Cryst. Liq. Cryst. **646**, 46–65 (2017). Copyright 2017 Author(s), licensed under a Creative Commons Attribution-NonCommercial-NoDerivatives (CC BY-NC-ND 4.0) license.

This reliance on specific molecular configurations, along with the bottleneck that rod-like molecular systems struggle to achieve stable macroscopic polarization, has long restricted the application of FLCs in broader photonic scenarios—after all, the core advantages of traditional NLCs lie in the universality and excellent hydrodynamic properties of rod-like molecules. If ferroelectricity cannot be realized in the nematic phase system, it will be difficult to combine the polarization modulation capability of FLCs with the integration compatibility of the nematic phase. For this very reason, the theoretical hypothesis of the "ferroelectric nematic phase"[72] proposed by Born in 1916 is of even greater groundbreaking significance: this hypothesis directly points to the possibility of ferroelectric polarization in rod-like molecular nematic phase systems, providing a theoretical anchor for breaking through the structural constraints of traditional FLCs. It was not until 2017 that the Mandle–Goodby research group in the UK and the Kikuchi research group in Japan independently discovered NLC materials with strong ferroelectric properties.[73,74] In 2020, the Clark team at the U.S. National Academy of Sciences provided direct experimental evidence of FNLCs, confirming their existence.[32] This milestone achievement, with its profound impact on soft matter science, was named one of *Physics World's* Top Ten Breakthroughs of 2020. Unlike the molecules in conventional NLCs, FNLCs exhibit a range of unique properties, including ultrahigh spontaneous polarization density, a dielectric constant an order of magnitude higher than that of conventional crystals, anomalous viscoelastic behavior, and excellent nonlinear optical response.

From the perspective of molecular orientational distribution, the polarization characteristics of conventional nematic LCs and FNLCs can be theoretically distinguished. In conventional nematic phases, molecular dipole moments are statistically symmetric along the long axis, leading to head–tail equivalence. Consequently, the overall macroscopic polarization vanishes, and the nematic remains nonpolar. By contrast, in FNLCs the molecular head and tail are no longer equivalent, and dipole moments spontaneously align along the director. This alignment breaks centrosymmetry and induces a long-range polar order, giving rise to a stable ferroelectric polarization state.

From a theoretical perspective, Born was the first to propose that the isotropic–nematic transition can be regarded as a transformation from a "quasi-ferroelectric" to a fully "ferroelectric" state, which can be described within a mean-field framework analogous to the Langevin–Weiss theory.[72] Subsequently, Frank incorporated polarization order into the elastic free-energy density and demonstrated that in nematic systems lacking inversion symmetry, polar ordering is inherently coupled to splay deformations.[75] Building on this foundation, later studies suggested that spontaneous quadrupolar distortions may constitute a thermodynamically stable ground state within certain temperature ranges. In parallel, Palffy-Muhoray argued from the perspective of molecular conformation constraints that properly designed discotic molecules could exhibit nematic ordering with ferroelectric character.[76] Further work by Berardi and co-workers provided compelling evidence that even molecules without permanent dipole moments can form polar nematic phases if their terminal interactions are asymmetric.[77,78] When a moderate dipole moment is introduced along the molecular long axis, the FN phase can be stabilized. However, excessively strong dipoles disrupt long-range polar order, favoring the emergence of complex local polar-domain structures.

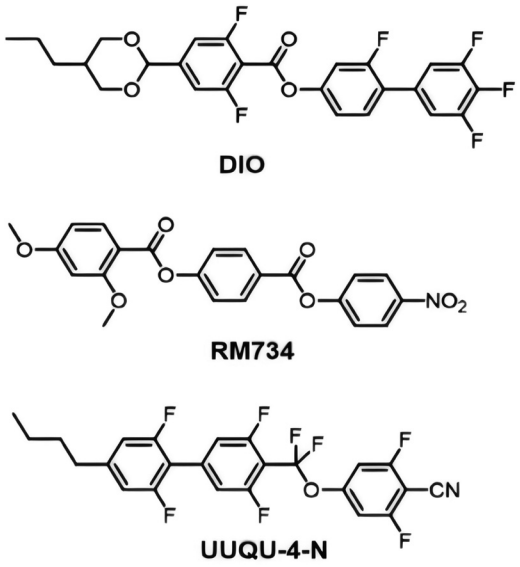

FIG. 6. Representative molecular structures of FNLCs: DIO, RM734, and UUQU-4-N.

As shown in Fig. 6, typical FNLC molecular structures can be broadly categorized into three main classes: (i) fluorinated molecules with dioxane–alkyl terminal groups, exemplified by DIO;[74] (ii) pear-shaped diester molecules such as RM734;[73,79] and (iii) recently developed highly fluorinated compounds such as UUQU-4-N,[80] characterized by CF_2O bridging groups and terminal cyano moieties. A common feature of these molecular designs is the presence of a pronounced dipole moment aligned along the molecular long axis, which is the key structural factor underpinning the stabilization of ferroelectric nematic phases.

In the Langevin–Weiss type mean-field framework, the ferroelectric phase arises from the cooperative alignment of molecular dipoles mediated by long-range dipole–dipole interactions. The material is assumed to be a dipolar liquid composed of molecules with dipole moments $\mathbf{p}$. The local electric field $\mathbf{E}_{\mathrm{loc}}$ acting on an individual dipole is not simply the external field $\mathbf{E}_0$, but rather the superposition of the external field and the reaction field generated by surrounding dipoles. This can be expressed as

$$\mathbf{E}_{\mathrm{loc}} = \mathbf{E}_0 + \alpha \mathbf{P}, \tag{1}$$

where $\mathbf{P}$ denotes the macroscopic polarization and α is the depolarization factor that depends on the assumed cavity model. The resulting torque on a dipole causes that the molecules tend to orient along the local field, which can be described in terms of the potential energy U

$$U = -\mathbf{p}\mathbf{E}_{\mathrm{loc}} = -pE_{\mathrm{loc}} \cos \beta, \tag{2}$$

where β is the angle between the dipole moment and the local field direction. Within the liquid state, dipoles are able to rotate freely; however, when an external field is applied, they tend to align along the local field direction for a finite period. The probability of a given dipole orientation follows the Boltzmann distribution: $\frac{1}{A}\exp(\mathbf{p} \cdot \mathbf{E}_{\mathrm{loc}}/(k_B T))$

with normalization constant $A = \int \exp(\mathbf{p} \cdot \mathbf{E}_{\text{loc}}/(k_B T))d\Omega$ where integration is performed over the entire solid angle Ω. The average polarization P is therefore expressed as

$$P = \rho_N p \langle \cos \beta \rangle, \tag{3}$$

where ρ_N is the number density and $\rho_N = \frac{N}{V}$. By defining $T_0 = \rho_N \alpha p^2/(3k_B)$ and $x = \alpha p P/(k_B T)$, Eq. (3) becomes

$$\frac{T}{3T_0} x = L(x), \tag{4}$$

where $L(x)$ is the Langevin function and $L(x) = \coth(x) - 1/x$. This equation gives a real solution for x when the temperature T is lower than T_0. So this model predicts that at T_0, the system undergoes the transition to the polar phase and below this temperature, and it exhibits spontaneous polarization $P = k_B T x_T/(\alpha p)$ where x_T is the solution of Eq. (4) at temperature T.

In Eq. (1), the contribution $\alpha \mathbf{P}$ to the local field is a sum of the dipolar fields of the surrounding molecules. In the mean field approach, α is the depolarization factor, which for a spherical cavity is equal to $1/(3\varepsilon_0)$. This is the value that Born took. However, the magnitude of the dipolar field decreases as r^{-3}, so on a given molecule, the nearest neighbors are those that contribute the most to the field. Moreover, because of the anisotropy of the dipolar field, the local field will strongly depend on the relative positions and orientations of the neighbors. In magnetic dipolar liquids, the simple mean field approach has been shown to overestimate the local field and the question of whether the dipolar interaction alone can lead to polar order remained unanswered.[81] On the other hand, the shape of the constituents can strongly affect the positional and orientational correlations between neighbors, and thus, it can promote or prevent the formation of the polar phase. A dipolar liquid made of plate-like constituents is more likely to exhibit a polar nematic phase than the one made of rods.[82]

C. Optical anisotropy and birefringence

Optical anisotropy is one of the most fundamental and indispensable physical properties of LC materials. More importantly, it serves as the core foundation for the wide application of LCs in photonic devices. This unique property originates from the intrinsic structural anisotropy of LC molecules—molecules are typically rod-shaped or disk-shaped, with asymmetric distributions of electron clouds and functional groups, leading to inherent differences in the optical responses of individual molecules along different molecular axes.

The birefringence of LC materials[83] is a direct manifestation of their optical anisotropy and also the physical basis for constructing various electro-optical devices. When unpolarized light is incident on an LC medium, the anisotropic arrangement of LC molecules splits the light beam into two orthogonally polarized beams, namely, ordinary light (o-light) and extraordinary light (e-light). These two beams propagate at different speeds in the medium, corresponding to refractive indices n_o (refractive index of o-light) and n_e (refractive index of e-light), respectively. The difference between them, $\Delta n = n_e - n_o$, is referred to as the birefringence, which is a key parameter characterizing the strength of the optical anisotropy of LCs. Thanks to their intrinsic birefringence, LC materials can effectively modulate the polarization state and phase of incident light. By precisely controlling the phase retardation between e-light and o-light, linearly polarized light can be converted into elliptically polarized light or circularly polarized light, or its polarization direction can be rotated.

Based on the sign of dielectric anisotropy ($\Delta\varepsilon = \varepsilon_{\parallel} - \varepsilon_{\perp}$), LC materials can be classified into positive LCs and negative LCs. Positive LCs exhibit a positive dielectric anisotropy, where the dielectric constant along the molecular long axis ($\varepsilon_{\parallel}$) is greater than that perpendicular to the long axis ($\varepsilon_{\perp}$), so the molecules align along the direction of the external electric field. In contrast, negative LCs have a negative dielectric anisotropy ($\varepsilon_{\perp} > \varepsilon_{\parallel}$), and the molecules align perpendicular to the external electric field.

D. Stimuli responsiveness

Another fundamental property of LC materials is their pronounced sensitivity to external stimuli, including electric, magnetic, thermal, mechanical, and optical fields. The molecular orientation and ordering of LCs can be reversibly reconfigured under these perturbations, enabling dynamic modulation of their optical properties.

For instance, in positive LCs, the molecular alignment can be continuously deflected by an applied electric field. As illustrated in Fig. 7, variations in the molecular tilt angle result in significant modulation of the effective refractive index.

Among these stimuli, electric fields represent the most widely employed control mechanism.[21,22] Many LC molecules possess permanent dipole moments or can induce polarization under an external field, thereby experiencing an electrostatic torque that drives molecular reorientation. For example, in nematic LCs, an applied parallel field reorients the director from its initial planar alignment to the field direction, altering birefringence and consequently modulating light transmission.

Magnetic field control,[23,24] by contrast, relies on anisotropic magnetic susceptibility. Although the required field strengths are typically higher than in electric control, magnetic fields minimally disturb LC microstructures. This feature makes them attractive for high-precision, non-contact photonic applications such as magnetically tuned phase retarders and magneto-optical modulators.

Thermal stimuli[25–27] also exert strong influence. Temperature variations affect intermolecular potentials, phase stability, and molecular order. In cholesteric LCs, heating increases the helical pitch, redshifting the selective reflection band, while in nematics, birefringence decreases

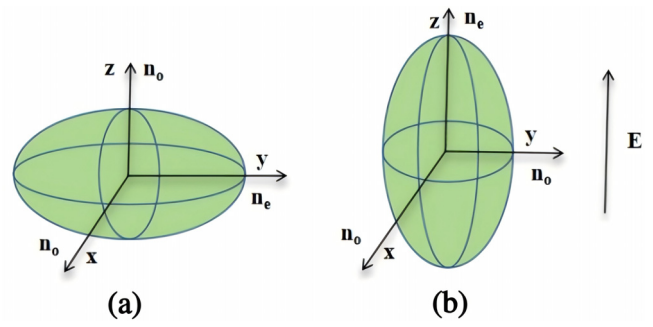

FIG. 7. Molecular alignment of positive NLCs: (a) field-off state and (b) field-on state.

as the clearing point is approached. Such effects enable thermochromic displays, thermal switches, and intelligent temperature sensors.

Mechanical responses arise from the viscoelastic nature of LCs. Shear flow, for instance, strongly reorients nematic molecules, inducing local ordering even in the isotropic phase and introducing biaxial symmetry across transitions. This coupling between mechanical stress and optical response provides a foundation for flexible photonic devices and strain-sensitive sensors.

Finally, optical fields[28] can directly reconfigure the LC orientation through photoinduced alignment or light absorption-driven thermal effects. These processes modulate refractive index distributions dynamically, underpinning phenomena such as optical self-focusing, all-optical switching, and holographic grating formation. Such photoresponsive nonlinearities highlight the promise of LCs for all-optical signal processing.

In summary, the inherent molecular anisotropy, diverse phase behaviors, and exceptional field sensitivities of LCs form the physical foundation for their broad applications in nonlinear optics and quantum photonics.

III. LIQUID CRYSTAL-ENABLED NONLINEAR OPTICS

This section focuses on the application of LCs in nonlinear optics, with an emphasis on the core advantages of FNLCs. By leveraging their spontaneous polarization properties and flexible molecular alignment control, FNLCs exhibit significantly enhanced second-order nonlinear effects. Moreover, their helical derivatives further optimize the nonlinear optical response by strengthening the polarization control dimension, giving rise to the innovative concept of "nonlinear geometric phase."

A. Optical nonlinearity of traditional liquid crystals

The origins of nonlinear optics can be traced back to the late 19th century. In 1875, Kerr reported a change in the refractive index of carbon disulfide (CS_2) under a strong electric field, a phenomenon that later became known as the electro-optic Kerr effect.[84] In 1893, Pockels systematically described another related effect in quartz crystals—the linear electro-optic effect (Pockels effect), where the refractive index varies linearly with the applied electric field.[85] These early discoveries provided the first proof that the optical properties of materials could be controlled by external fields. With the invention of the ruby laser by Maiman in 1960, the field underwent a paradigm shift: the laser provided a strong, coherent light source for exploring nonlinear interactions. Just a year later, Franken and Ward observed SHG in quartz,[86] an experiment widely regarded as the starting point of modern nonlinear optics. Subsequently, Bloembergen *et al.* developed a theoretical framework for the nonlinear polarization of dielectrics, introducing higher-order susceptibilities [$\chi^{(2)}$, $\chi^{(3)}$, …] to describe the microscopic origins of nonlinear responses.[87] This foundation quickly expanded to organic systems: in 1964, Rentzepis and Pao achieved SHG in pyrene molecules;[88] around 1970, Davydo *et al.* observed strong second-order nonlinear responses in π-conjugated molecules used as electron acceptors.[89] These milestones not only laid the physical groundwork for nonlinear optics but also spurred the development of both inorganic and organic nonlinear optical materials, while the Lorentz oscillator model further connected classical mechanics with nonlinear optical phenomena. Despite these advances, the application of traditional inorganic crystals and organic molecules in flexible photonics and integrated platforms remains limited by high production costs, mechanical brittleness, and insufficient flexibility. This has led researchers to focus on LC materials, which offer adjustable structures and performance advantages.

The nonlinear optical characteristics of LCs can be achieved through doping. By introducing guest materials with special optical responses into the LC matrix, the excellent compatibility of LCs with the doped phase can enhance the system's nonlinear polarization, significantly improving the nonlinear optical properties.

Currently, researchers have attempted to introduce various doping materials into LC matrices. For example, in studies involving metal nanoparticles, researchers dispersed silver and gold nanoparticles in phthalocyanine-based or nematic LCs, and found that under 532 nm nanosecond laser pulses, metal nanoparticles could enhance the nonlinear optical absorption properties of the LC system.[90] Further investigation using Z-scan techniques showed that gold nanoparticles doping could effectively improve the nonlinear refractive properties of LCs, with the nonlinear refractive index n_2 increasing as the concentration of gold nanoparticles increased. The properties could also be modulated by electric and optical fields.[91,92] Additionally, characterization of nematic LC (6CHBT) and its mixtures with polyaniline and silver nanoparticles revealed that the doping materials had a significant effect on the thermodynamic, dielectric, and electro-optic parameters of the pure LC.[93]

In the field of semiconductor nanoparticle doping, research teams doped TiO_2 nanoparticles into nematic LCs, and experiments confirmed that the dielectric constant of the doped composite system was higher than that of pure nematic LCs.[94] Studies on CdSe and ZnS quantum dot-doped LCs showed that these doping systems significantly enhanced the optical nonlinearity, making them potential candidates for optical limiting applications.[95,96] In the field of carbon nanomaterial doping, studies on the third-order NLO properties of graphene oxide (GO) doped LC systems showed that the optical refractive index, third-order nonlinear refractive index, and absorption coefficient increased with GO doping. The incorporation of GO also enhanced the birefringence effect, nonlinear absorption, and nonlinear refraction (NLR), as well as two-photon absorption (TPA) effects. Under certain doping concentrations, the NLO parameters reached their maximum values.[97,98] Z-scan measurements of single-walled carbon nanotubes (SWCNTs) and graphene-doped 8CB LC systems showed that the NLO properties of the doped LC systems were enhanced as the concentration of SWCNTs and graphene varied. At certain doping concentrations, the composite system exhibited optimal third-order NLO performance.[99,100] Moreover, research on carbon dot (c-dot) doped nematic LCs confirmed that the NLO properties of the doped system were significantly improved, with excellent optical limiting thresholds at specific doping concentrations.[101]

In addition to doping modification, laser induction is another major technique for stimulating the nonlinear properties of LCs. As an external field stimulus, laser light can induce macroscopic molecular reorientation through photo-orientation effects, triggering NLO responses caused by changes in molecular order. In studies investigating the laser excitation of LC nonlinear properties, a variety of explorations have been conducted. In 2003, an LC material containing a TPA chromophore was shown to generate upconverted fluorescence in the visible light range under 800 nm strong infrared pulse laser excitation, exhibiting excellent optical limiting effects and stability under 815 nm, 5 ns pulse laser exposure.[102] In 2007, a research team excited E7 LCs

with a femtosecond titanium sapphire laser (pulse width 70 fs, repetition rate 80 MHz, etc.), resulting in SHG.[103] Another study involved using 7CB as the base material, doped with the two-photon dye MBAPB, to prepare dye-doped LC materials. Under continuous 1064 nm laser excitation, the system exhibited photo-induced fluorescence through two-photon absorption.[104]

As the technical path continues to be optimized, device structure innovation has become a key direction for further breaking through the NLO performance limits of LCs. In 2023, a research team adopted a multi-layer composite structure to prepare NLO devices from multi-wall carbon nanotube/LC composite systems. Z-scan testing showed that the third-order nonlinear polarization of the device was approximately five times higher than that of traditional devices, and its performance could be further enhanced by nearly 31% under applied voltage. The unique electro-tunable characteristics of this device open new technical pathways for the fabrication of NLO devices.[105]

B. Nonlinear properties enabled by ferroelectric nematic liquid crystals

Compared to conventional LC phases, FNLCs can maintain an effective second-order nonlinear polarization tensor even under the lowest symmetry point group ($C_{\infty v}$), making them highly promising as tunable, processable, and flexible NLO materials.

Under this symmetry condition, the second-order nonlinear susceptibility is more commonly characterized using a 3×6 order $d_{\alpha\beta}$ matrix [where $\alpha = 1, 2, 3$ corresponds to the component of the polarization direction, and $\beta = 1$–6 corresponds to the 6 independent combinations of electric field components: $(11) \rightarrow 1, (22) \rightarrow 2, (33) \rightarrow 3, (23/32) \rightarrow 4, (13/31) \rightarrow 5, (12/21) \rightarrow 6$]. The relationship between $\chi^{(2)}_{ijk}$ and $d_{\alpha\beta}$ satisfies $\chi^{(2)}_{ijk} = 2d_{i\beta}$ (where β matches the combination of j, k, so the expanded form of $\chi^{(2)}_{ijk}$ is given by

$$\chi^{(2)}_{ijk} = 2\begin{pmatrix} 0 & 0 & 0 & 0 & d_{15} & 0 \\ 0 & 0 & 0 & d_{24} & 0 & 0 \\ d_{31} & d_{32} & d_{33} & 0 & 0 & 0 \end{pmatrix}. \quad (5)$$

Here, the z axis corresponds to the polarization direction of the electric field, while the x and y axes are equivalent. For such a nonlinear system, the relations $d_{31} = d_{15} = d_{32} = d_{24}$ hold, reducing the tensor to only two independent coefficients. Substituting $\chi^{(2)}_{ijk}$ into the expression of the second-harmonic polarization $P_i^{(2\omega)} = \varepsilon_0 \chi^{(2)}_{ijk} E_j E_k$ yields

$$\begin{bmatrix} P_x \\ P_y \\ P_z \end{bmatrix} = 2\varepsilon_0 \begin{pmatrix} 0 & 0 & 0 & 0 & d_{31} & 0 \\ 0 & 0 & 0 & d_{31} & 0 & 0 \\ d_{31} & d_{31} & d_{33} & 0 & 0 & 0 \end{pmatrix} \cdot \begin{pmatrix} E_x E_x \\ E_y E_y \\ E_z E_z \\ 2E_z E_x \\ 2E_x E_z \\ 2E_x E_y \end{pmatrix} = \begin{pmatrix} 4\varepsilon_0 d_{31} E_x(\omega) E_z(\omega) \\ 4\varepsilon_0 d_{31} E_y(\omega) E_z(\omega) \\ 2\varepsilon_0 d_{31} E_x(\omega)^2 + 2\varepsilon_0 d_{31} E_y(\omega)^2 + 2\varepsilon_0 d_{33} E_z(\omega)^2 \end{pmatrix}. \quad (6)$$

In FNLCs, the spontaneous polarization primarily arises from the asymmetric stacking of molecules driven by dipole–dipole interactions, which disrupts the macroscopic inversion symmetry. In this structure, the molecular dipoles align strongly along the director, giving the material significant polar anisotropy. The chromophores with nonlinear optical activity, acting as dipole sources, are typically aligned with the molecular long axis and are consistent with the polarization direction of the FNLCs. This synergistic structural effect effectively enhances the second-order nonlinear response, with the equivalent nonlinear coefficient being several orders of magnitude higher than that of traditional FLC systems.

To quantitatively evaluate the nonlinear optical properties of FNLCs, researchers have systematically characterized them using the Maker fringe technique.[106] The results indicate that the equivalent second-order nonlinear optical coefficient of some FNLCs can reach ~1–20 pm/V, which is significantly higher than that of traditional FLC systems. Based on these findings, researchers proposed a set of universal molecular design principles and introduced machine learning algorithms for intelligent screening and optimization of high-polarization FNLC materials.

To verify these theoretical predictions, a research team adopted a combined experimental approach using POM, SHG testing, and dielectric spectroscopy analysis to systematically explore the structural characteristics and physical properties of novel polar nematic LCs. The experimental results confirmed that such polar nematics are widely present in rod-like molecular systems, and their formation mechanism is closely related to the dynamic evolution of topological defects. The thermodynamic stability of polarization domains provides crucial support for the maintenance of the phase structure. This discovery further refines the formation theory of polar nematics and reveals the core principles of the synergistic effect between molecular ordering and polarity. Importantly, the research team successfully identified a class of molecular materials that combine high dielectric constant and strong second-order NLO response.

Building on these findings, the research team extended the design principles of polar nematics to polymer systems (as shown in Fig. 8), achieving a transition from small molecules to polymer materials in the application scenarios of polar LCs. The synthesized side chain polymer LCs exhibit typical FNLC characteristics and orientation textures due to the ordered arrangement of molecular segments. Moreover, the polymer LCs maintain a significant SHG response even in the absence of an external field, confirming the stability and tunability of the polar nematic structure in polymer systems. This breakthrough not only expands the material boundary of FNLCs but also provides new possibilities for their application in flexible optoelectronic devices, wearable photonic devices, and other emerging fields, further verifying the feasibility and potential value of their large-scale applications.

C. Enhanced nonlinear effects enabled by helical ferroelectric nematics

The existence of helical FNLCs was first experimentally confirmed.[107] As shown in Fig. 9, in this novel phase, the polar molecules are arranged along a helical path, with their polarization vectors forming a spatially helical distribution, exhibiting an electrical analog of a helimagnetic structure. This phase not only remains stable at room

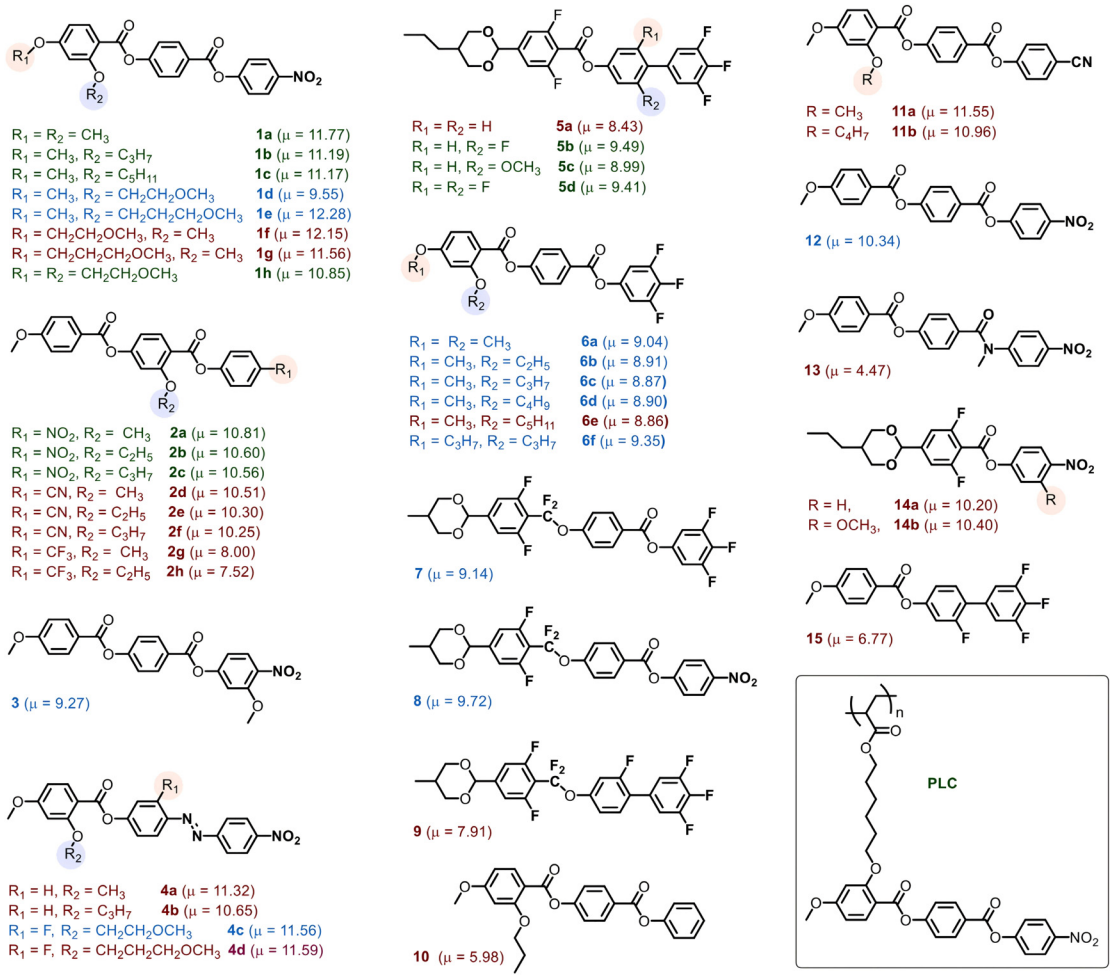

FIG. 8. Molecular library of synthesized compounds. The figure displays all synthesized materials with dipole moment values calculated using density functional theory. Compounds marked in green exhibited stable nematic alignment during cooling. Blue labels indicate unstable nematic phases observed, while red labels denote compounds where no nematic phase was observed at any temperature during cooling.[106] Reproduced with permission from Li *et al.*, Sci. Adv. **7**, eabf5047 (2021). Copyright 2021 Author(s), licensed under a Creative Commons Attribution (CC BY 4.0) license.

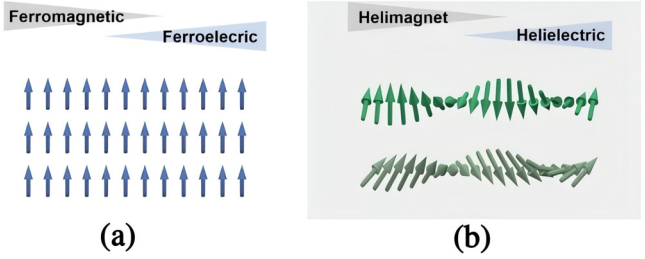

FIG. 9. Electric and magnetic states. (a) Uniform magnetization or polarization. (b) Helimagnetic or helielectric states. The possible helical (top) and anti-helical (bottom) textures are shown.[107] Reproduced with permission from Zhao *et al.*, Proc. Natl. Acad. Sci. U. S. A. **118**, e2111101118 (2021). Copyright 2021 Author(s), licensed under a PANS license.

temperature but also exhibits significantly enhanced dielectric responses and second-order NLO characteristics.

By combining SHG interference microscopy, the "head-to-tail" orientation of the polar molecules was directly observed, and the polarization vector could be reversibly controlled by applying an external electric field. Additionally, studies have shown that under optimized chiral dopant concentrations, the SHG signal intensity could be effectively enhanced, with a maximum enhancement of ~500 times.

More importantly, the pitch length of this phase can be precisely tuned within a range from micrometer scales to near-ultraviolet wavelengths, greatly expanding its application prospects in wavefront modulation and nonlinear photon control. Furthermore, the reversible transition between the polar helical nematic phase and the nonpolar helical nematic phase not only enriches the phase dynamics of soft matter systems but also provides an ideal platform for exploring topological phenomena in such systems. Building on these unique

advantages—including broadband pitch tunability and reversible phase switching—future research should focus on stabilizing helical polar structures through polymer network modification, while achieving low-voltage reversible control over their optical properties. These efforts will lay a critical foundation for realizing compact, flexible, and integrable nonlinear photonic devices, thereby unlocking their full potential in next-generation quantum optics, ultrafast photonics, and on-chip photonic integration.

D. Nonlinear geometric phase in ferroelectric nematics

In modern photonics, the simultaneous manipulation of multiple degrees of freedom (DoFs) of light is regarded as a critical objective. Nonlinear wavefront shaping offers a powerful approach by converting an incident beam into a frequency-converted output that exhibits spatially variant phase, amplitude, and orbital angular momentum, thereby enabling multidimensional information control. Nevertheless, achieving reconfigurable control of structured light fields in high-order, multimode nonlinear photonic systems remains a formidable challenge.

To address this bottleneck, a novel concept of nonlinear geometric phase based on ferroelectric materials has recently been proposed.[36] Here, the nonlinear geometric phases emerge during second-order polarization process. For an LC director rotated by an angle α around the z axis, the Second-harmonic wave (SHW) acquire nonlinear geometric phases of $\sigma\alpha$ (co-circular) and $3\sigma\alpha$ (cross-circular), where $\sigma = \pm 1$ is the spin angular momentum state. The origin of the nonlinear geometric phase in the FNLC can be explained as follows. The second-order susceptibility is defined locally as $\vec{\vec{\chi}}^{(2)}(0) = \vec{\vec{\chi}}^{(2)}(\alpha)|_{\alpha=0}$, and the SHW is calculated as

$$P^{2\omega} = \varepsilon_0 \vec{\vec{\chi}}^{(2)}(0)\left(\mathbf{E}^{\omega}_{\mathrm{Local}}\right)^2 = \varepsilon_0 \chi^{(2)}_{\mathrm{aaa}}\left(\mathbf{E}^{\omega}_{\mathrm{Lab}}\right)^2 e^{2i\sigma\alpha}. \tag{7}$$

After transforming back to the laboratory frame, the nonlinear polarizations with co- and cross-circular polarization to that of the fundamental wave (FW) are derived

$$\begin{aligned} P^{2\omega}_{\sigma} &= \varepsilon_0 \chi^{(2)}_{aaa}(E^{\omega}_{\sigma})^2 e^{2i\sigma\alpha} e^{-i\sigma\alpha} \propto e^{i\sigma\alpha}, \\ P^{2\omega}_{-\sigma} &= \varepsilon_0 \chi^{(2)}_{aaa}(E^{\omega}_{\sigma})^2 e^{2i\sigma\alpha} e^{i\sigma\alpha} \propto e^{3i\sigma\alpha}. \end{aligned} \tag{8}$$

This mechanism exploits the spin-dependent nonlinear phase response inherent in second-order nonlinear polarization processes to dynamically tailor the wavefront of nonlinear optical fields. As a proof-of-concept, a photo-patterned FNLC q-plate was fabricated, exhibiting cascaded linear and nonlinear spin–orbit coupling effects. This configuration enabled the generation of SH optical vortices with spin-locked topological charges. It is worth noting that for the linear spin–orbit interaction during the propagation of SHW, the angular momentum states remain spin-locked.

As illustrated in Fig. 10, the second-order nonlinear polarization process in the FNLC medium imparts distinct nonlinear geometric phases to left- and right-circularly polarized components, resulting in a highly controllable nonlinear interference field. Furthermore, through spatial engineering of the polar director configuration, these geometric phases can be continuously tuned, thereby enabling precise and versatile wavefront shaping capabilities.

When a fundamental wave with the spin and orbital angular momentum states of $(\sigma, l_0)_{\omega}$ is incident on the ferroelectric, the cascaded spin–orbit interactions will generate two spin–orbit-locked second-

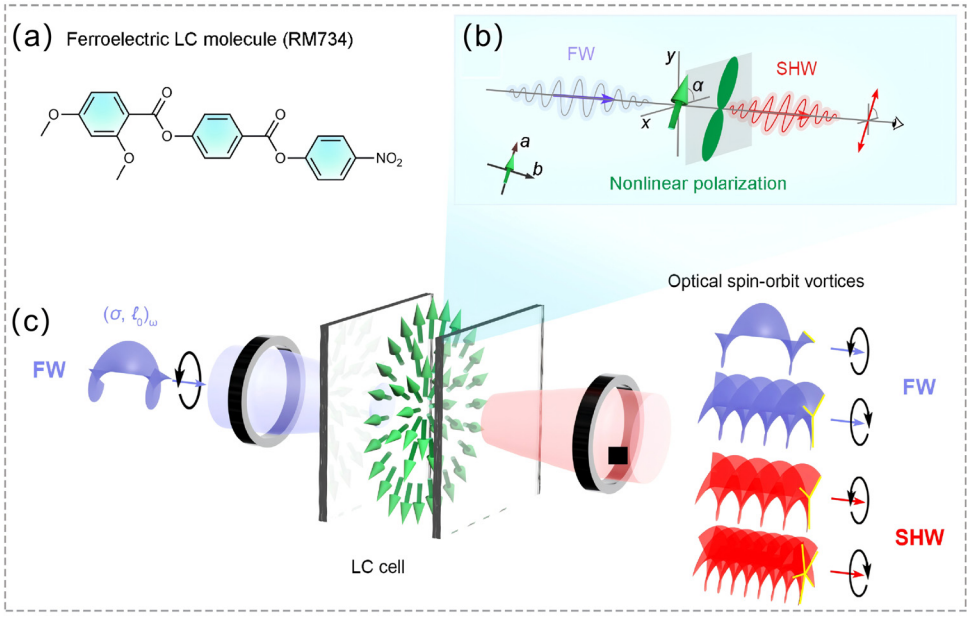

FIG. 10. (a) Chemical structure of RM734. (b)SHW generated from the polar RM734 material under the pumping of linearly polarized fundamental wave (FW). The nonlinear polarization direction of the LC is consistent with the polar direction. (c) Spin-orbit angular momentum states of multiple SHWs generated in a nonlinear LC q-plate. When the incident FW has an angular momentum state of $(\sigma, 0)_{\omega}$, the SHW will possess specific angular momentum states due to the spin–orbit interaction between the FW and SHW, where $\sigma = \pm 1$ represents the circular polarization state of light.[36] Reproduced with permission from Pan *et al.*, Nat. Commun. **15**, 8732 (2024). Copyright 2024 Author(s), licensed under a Creative Commons Attribution (CC BY 4.0) license.

harmonic optical vortices $(-\sigma, 2l_0 + \sigma q)_{2\omega}$ and $(-\sigma, 2l_0 + 3\sigma q)_{2\omega}$, as well as two fundamental optical vortices $(-\sigma, l_0 + 2\sigma q)_{\omega}$ and $(\sigma, l_0)_{\omega}$.

A remarkable feature of this nonlinear geometric phase is its high degree of external tunability. By adjusting physical parameters such as temperature, applied electric fields, and twist elastic constants, the morphology of SH structured beams can be modulated in real time, offering promising opportunities in optical communications, quantum information processing, and high-resolution imaging.

Building on this, a research team further focused on the key requirement of "dynamic reconfigurability," advancing the study from "feasibility verification of nonlinear optical field control" to "real-time tunable functionality implementation." They optimized the film quality of FNLCs through ion doping and introduced an in-plane electric field control strategy, constructing a reconfigurable nonlinear Pancharatnam–Berry phase optical system.[35]

The soft-matter FNLC platform and its nonlinear geometric-phase mechanisms both deepen our basic understanding of dynamic light–matter coupling in nonlinear optics and point to a practical route for reconfigurable, low-footprint nonlinear photonics. In summary, FNLCs uniquely combine large, switchable $\chi^{(2)}$ with programmable nonlinear geometric phase distribution, enabling electrically and optically programmable functions such as vortex beam generation, nonlinear holography, super-resolution contrast enhancement, and routes to quantum state conversion.

IV. LIQUID CRYSTAL-ENABLED QUANTUM OPTICS

Owing to their excellent NLO properties, flexible tunability under external fields, and high integration potential, LCs have been incorporated into a variety of quantum optical systems.[106] Among them, FNLCs are particularly prominent: they exhibit outstanding quantum frequency-conversion performance, and their unique macroscopic polarization structure combined with precisely tailorable molecular configurations provides an ideal soft-matter platform for the efficient generation and manipulation of complex entangled photon states.

This section focuses on the role of LCs in quantum optics, with particular emphasis on recent advances and application prospects of FNLCs in correlated photon-pair generation and precise control of tunable entangled states. These efforts aim to further extend the physical boundaries and functional capabilities of LC-based materials in quantum information processing and quantum devices.

A. Applications of traditional liquid crastal elements in quantum optics

Vector vortex beams (VVBs) have attracted widespread interest in both classical and quantum optics. In such beams, the linear polarization state varies periodically with the azimuthal angle of the optical vortex around the beam axis, giving rise to a characteristic phase singularity. VVBs are therefore among the most widely used classes of vector beams in current research.[108–111] The geometry of generalized VVBs is often described using higher-order or hybrid-order Poincaré spheres,[112–114] which provide higher degrees of freedom than scalar vortex beams or purely vector beams. Importantly, vector vortex modes serve as eigenmodes of optical fibers and thus exhibit robust propagation properties.[115,116] They can significantly increase the capacity of optical communication systems[117] and find important applications in beam focusing, particle acceleration, vector-vortex filtering, materials processing, and quantum information processing.[118–121] As a result, techniques for the efficient generation and precise control of vector beams have become a central research topic.

A q-plate (also referred to as a vortex phase retarder) is one of the most commonly used optical elements for generating vector beams.[122] Essentially, a q-plate is a birefringent waveplate whose local optical axis in the transverse plane is spatially inhomogeneous, with the distribution pattern defined by its topological charge q (which can be an integer or half-integer). In practical implementations, q-plates are typically operated as half-wave, electrically tunable retarders to achieve efficient conversion at a target wavelength. When a circularly polarized beam is incident on a q-plate, the output beam acquires an orbital angular momentum (OAM) of $2q\hbar$, with the sign determined by the helicity of the incident polarization.[123–127] Figure 11 illustrates the geometric structures of three representative q-plates and summarizes their action on circularly polarized beams, thereby establishing q-plates—often realized as LC-based Pancharatnam–Berry phase elements—as key enabling components for vector-beam applications in the quantum domain.

LC-based q-plates play a central role in quantum optics. This subsection focuses on their concrete applications in the generation of various entangled structures and in two-photon interference. LC q-plates can be used directly to prepare nonseparable states in quantum systems.[128,129] The defining feature of a vector field is the coupling between polarization and spatial mode: unlike scalar fields, these two degrees of freedom are nonseparable. This property is commonly described in terms of *classical entanglement* or *intra-system entanglement*; its mathematical structure is equivalent to that of quantum entanglement, but it does not involve nonlocal correlations between distinct physical subsystems. In studies of the state evolution of classically entangled degrees of freedom in atmospheric turbulence,[130] q-plates have already been used to encode and decode entangled qubits. In combination with a spatial light modulator (SLM), they have also enabled measurements of the nonseparability of vector-vortex modes, providing important experimental support for the use of LC devices in practical quantum control.

Building on this technical foundation, Parigi *et al.* employed patterned LC q-plates to demonstrate the storage and retrieval of single-photon-level vector beams in a laser-cooled atomic ensemble.[131] In their protocol, q-plates are used for both state preparation and readout: the generated vector state is first converted into a purely polarization-encoded state, which is then analyzed using a second q-plate together with standard polarization optics. Similarly, Li *et al.* used an SLM to realize the storage of hybrid-entangled single-photon states in a solid-state medium,[132] further expanding the range of quantum-state manipulations enabled by LC-based devices.

For the control of entangled photon pairs, researchers have combined SPDC-generated entangled photons with VVBs produced by q-plates. D'Ambrosio's group systematically investigated two types of entangled VVBs[133] and confirmed that these complex polarization structures represent a direct manifestation of intra-system entanglement between polarization and OAM. By contrast, inter-system entanglement between two vector fields can be exploited in a broader set of quantum protocols and therefore warrants further study. At the same time, this approach has already been pushed toward field deployment: a metropolitan free-space link in Ottawa has been used to test high-dimensional quantum key distribution outside the

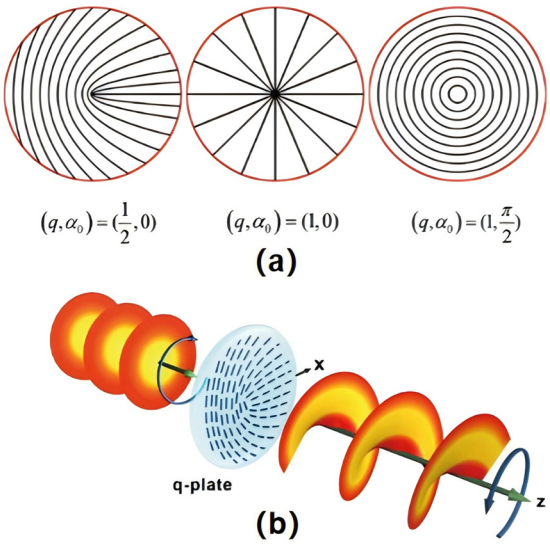

FIG. 11. (a) Three examples of *q*-plate patterns with α_0 being the initial optical axis orientation,[123] Reproduced with permission from Marrucci *et al.*, Phys. Rev. Lett. **96**, 163905 (2006). Copyright 2006 American Physical Society. (b) Illustration of the optical action of a q-plate with $q = 0.5$ on the left circularly polarized light beam.[124] Reproduced with permission from Ji *et al.*, Sci. Rep. 6, 25528 (2016). Copyright 2016 Author(s), licensed under a Creative Commons Attribution (CC BY 4.0) license.

laboratory, where LC q-plates were employed to prepare the initial quantum states.[134] In addition, a recent work proposed an efficient scheme for generating complex three-degree-of-freedom entangled light fields.[135] By combining time–frequency-mode (TFM) encoding in the SPDC process with VVB encoding via q-plates, the authors realized a structurally simple yet high-quality TFM–VVB hyperentangled source.

In recent years, SLM-mediated multiplexing of vector beams has attracted considerable interest[136–138] as a means of further increasing data transmission rates. Otte *et al.* demonstrated a practical implementation of this multiplexing technique for the generation and propagation of engineered optical fields.[139] By superposing two orthogonal vector beams, they generated a field whose local degree of entanglement varies along the propagation axis *z*. During free-space propagation, this field exhibits a characteristic evolution of local entanglement. In their experiment, digital propagation of the field was implemented using an SLM and lenses in a Fourier-transform configuration, thereby enriching the LC-based toolbox for quantum-field engineering. Chen *et al.* used uniformly self-assembled cholesteric LCs to realize logical rotations of nonseparable vector states by tuning the incidence angle of the beam, thus emulating core quantum-information operations. This approach provides a new paradigm for structured photonics that relaxes stringent real-space alignment requirements. Although the logical gate is implemented in a classical regime, applying the same operations to single photons or entangled states in quantum-information processing holds substantial promise.[140]

Beyond the generation and control of entangled states, LC devices also play an indispensable role in quantum-walk experiments, where they have been employed not only for simulating quantum dynamics[141–143] but also for the preparation of high-dimensional quantum states.[144–147] Experiments have demonstrated engineered preparation of arbitrary two-qubit states based on discrete-time quantum walks,[145] with the shift operator implemented using a sequence of five q-plates. Giordani later proposed an entanglement-transfer protocol based on quantum walks that enables the dynamic transfer of qubit–qubit entanglement from lower to higher dimensions,[146] highlighting the unique advantages of LC devices for flexibly generating high-dimensional entanglement.

LC-based devices are equally central in quantum-interference studies. The Hong–Ou–Mandel (HOM) effect, a paradigmatic two-photon interference phenomenon, is widely regarded as one of the most iconic signatures of quantum interference in optics: when two indistinguishable photons interfere at a beam splitter, they exhibit photon bunching or antibunching behavior. Because it has no classical analog, the HOM effect is of fundamental significance and serves as a key resource in precision metrology, quantum computing, and quantum communication.[148] LC optical elements provide convenient handles for tunable HOM interference. Q-plates have been used to demonstrate HOM interference between scalar OAM states.[149] By tuning two key parameters of a q-plate, researchers realized adjustable HOM interference between vector modes.[150] The transformation induced by the q-plate on VVBs can be visualized as trajectories on a hybrid Poincaré sphere. Progress has also been made on two-photon interference in high-dimensional mode spaces: in one experiment, three SLMs were used to implement spatial-mode generation, unitary transformations, and projective measurements, respectively.[151] Collectively, these studies underscore the broad and versatile role of LC devices in quantum-information processing tasks.

On the basis that LC devices have gradually covered various core scenarios of quantum information, including quantum entangled state manipulation, high-dimensional quantum walk simulation, and quantum interference effect control, the in-depth exploration of their topological regulation potential has become a key direction to drive breakthroughs in the field. The innovative strategy proposed by scholars such as Koni *et al.* recently is a landmark achievement in this exploration process—the team for the first time realized the

reconfigurable preparation and regulation of dual-wavelength quantum optical skyrmions mediated by LC topological defects, injecting a brand-new technical path into the field of topological quantum optics.[152]

This study employed a 532 nm continuous-wave laser to pump a type-0 non-degenerate SPDC crystal, generating collinear photon pairs at 1550 nm/810 nm that are entangled in both orbital OAM and wavelength degrees of freedom. Subsequently, a 10 μm thick nematic LC q-plate (with $q = 1$ intrinsic topological defect) induced by magneto-electric coordination was utilized to achieve voltage- and wavelength-dependent spin–orbit conversion. Combining OAM projection via single-mode fibers and polarization tomography technologies, a switchable quantum topological state platform was constructed. Experimental results demonstrate that this system can not only prepare dual-wavelength nonlocal entangled skyrmions with a skyrmion number of $N \approx -2$ at a voltage of 3.85 V (with an entanglement concurrence of 0.83, exceeding the entanglement threshold of 0.7), but also realize single-wavelength heralded single-photon skyrmions at 810 nm/1550 nm in the voltage range of 5.4–6.3 V, and switch to trivial topological states ($N \approx 0$) near 4.9 V. More importantly, these topological states exhibit strong robustness against transmission through complex media such as biological samples (e.g., butterfly wings). Theoretically, through wavelength-selective spin–orbit conversion and multi-dimensional projection, it is feasible to construct three-body GHZ-like entangled states across polarization, OAM, and wavelength, transforming the wavelength from a traditional independently separable degree of freedom into an intrinsically inseparable dimension of topological structures. This work not only breaks through the limitations of single-wavelength and non-switchable topological states of traditional quantum skyrmions, but also introduces intrinsic LC topological defects into quantum topological regulation for the first time. It provides a new technical paradigm for high-robustness quantum information encoding in optical fiber communication and biological imaging fields, further expands the application boundary of LC devices in quantum optics, and lays a core foundation for the engineering preparation and practical implementation of multi-degree-of-freedom topological quantum states in subsequent research.

B. Ferroelectric nematics enabled tunable entangled photon pairs

A 2024 study published in *Nature* reported the first realization of spontaneous parametric downconversion SPDC in an FNLC and demonstrated a multidimensionally tunable entangled photon-pair source, whose operating principle is sketched in Fig. 12. This work introduces a new paradigm for quantum photonics that combines high degrees of control with high generation efficiency. Experiments show that applying only a few volts across the FNLC cell, or introducing a slight twist in the molecular orientation, is sufficient to substantially modify both the emission rate and the polarization distribution of the photon pairs.

The underlying mechanism relies on a distinctive quasi-phase-matching strategy, rooted in the twisted molecular-scale director configuration of FNLCs. This internal twist enables dynamic reconfiguration of the spectral properties of the photon pairs and of the correlations between their polarization components, thereby providing a powerful route to engineer high-dimensional entangled states in a compact, low-power platform.

Electric-field-driven dynamic control is one of the most application-relevant features of this FNLC-based SPDC platform: by applying only a few volts across the FNLC cell, the molecules are reoriented along the field direction, enabling rapid switching of the polarization state of the entangled photon pairs. On this basis, the biphoton polarization state can be further reconstructed and analyzed. Unlike classical or single-photon polarization states, which can be expressed as superpositions of two orthogonal basis states (such as horizontal H

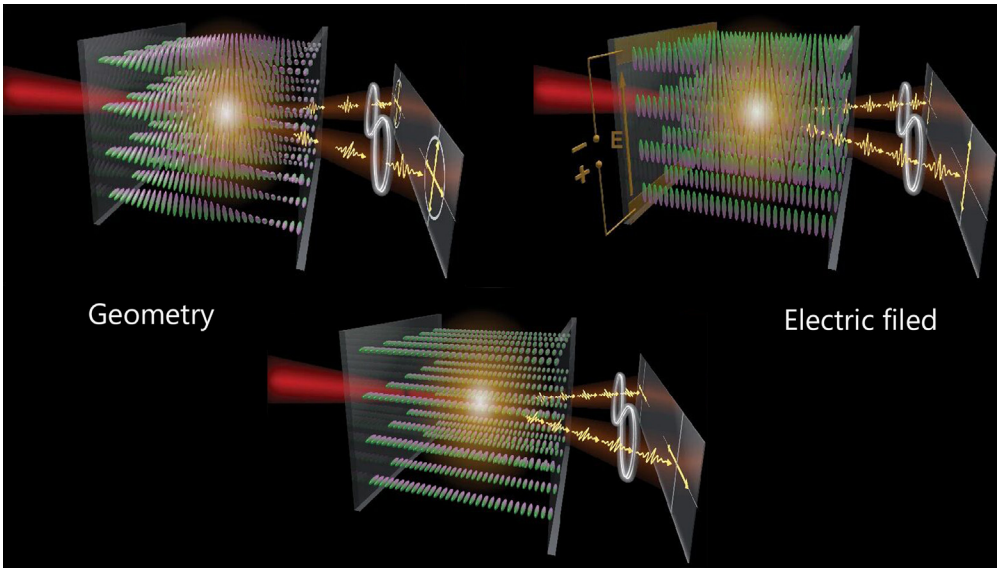

FIG. 12. Entangled photon generation in FNLC cells. The main concept of this study is: by reconfiguring the molecular alignment, both the photon pair flux and polarization state can be simultaneously controlled. This reconfiguration of the molecular alignment can be achieved by designing the sample geometry or applying an external electric field.[38] Reproduced with permission from Sultanov *et al.*, Nature **631**, 294–299 (2024). Copyright 2024 Author(s), licensed under a Creative Commons Attribution (CC BY 4.0) license.

and vertical V polarization), a two-photon polarization state must, in general, be described in the four-dimensional Hilbert space spanned by the corresponding two-photon polarization basis. However, when no degree of freedom other than polarization is used to distinguish the two photons, the effective state space reduces to a three-dimensional subspace, and the entangled two-photon polarization state can be written as

$$|\psi\rangle = C_1|2\rangle_H|0\rangle_V + C_2|1\rangle_H|1\rangle_V + C_3|0\rangle_H|2\rangle_V, \tag{9}$$

where C_1, C_2, and C_3 are complex amplitudes satisfying $|C_1|^2 + |C_2|^2 + |C_3|^2 = 1$, and $|N_p\rangle$ denotes a Fock state with N photons in polarization mode p. The corresponding density-matrix formalism naturally extends this description to mixed states. When the photon pairs are detected in a single, collinear spatial mode and their frequencies are not resolved, the two-photon polarization state is fully characterized by a 3×3 density matrix, which can be reconstructed by polarization tomography combined with maximum-likelihood estimation.

As shown in Fig. 13, with increasing applied electric field the reconstructed biphoton polarization state evolves from a state corresponding to two horizontally polarized photons, through intermediate superposition states, to a state corresponding to two vertically polarized photons. Further increasing the field strength does not induce any substantial additional change. Thus, by electrically reorienting the FNLC molecules, one can obtain two-photon polarization states composed of two H or two V photons, as well as any intermediate polarization state between these two limits.

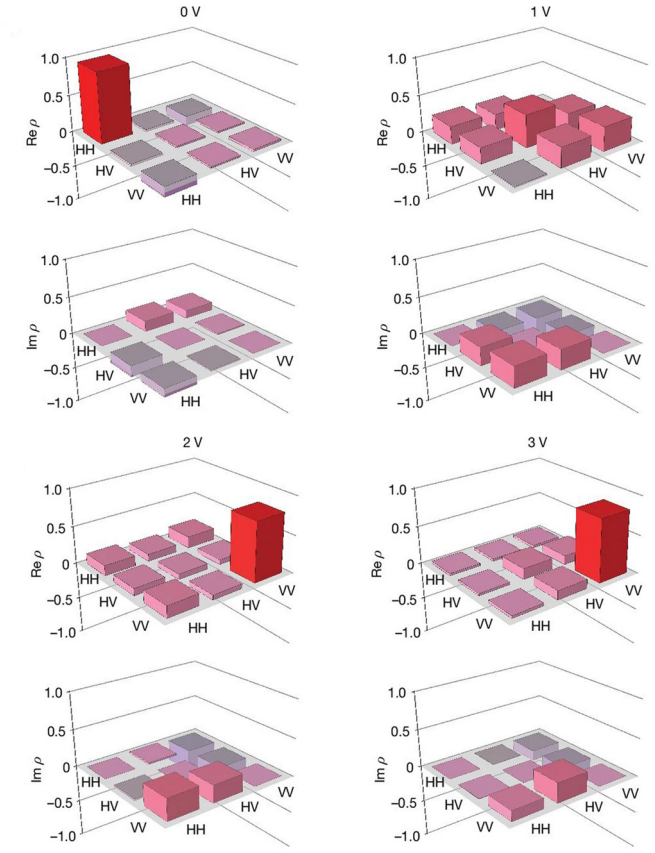

FIG. 13. Electric field-tuned SPDC process. The evolution of the polarization state can be observed through the reconstructed polarization density matrix at 0, 1, 2, and 3 V.[38] Reproduced with permission from Sultanov *et al.*, Nature **631**, 8020 (2024). Copyright 2024 Author(s), licensed under a Creative Commons Attribution (CC BY 4.0) license.

Static geometric control is achieved by predefining the twist angle of the FNLC director along the cell thickness (for example, 0, $\pi/2$, or π), thereby enabling precise engineering of the polarization entanglement. In a cell with zero twist, the molecular orientation is uniform, and the generated photon pairs are predominantly in a collinearly polarized state. In a $\pi/2$-twisted cell, the director gradually rotates from horizontal to vertical, and the photon pairs form a hybrid state in which vertically polarized pairs dominate, with a smaller contribution from cross-polarized (HV) components. In a π-twisted cell, the molecular orientation symmetrically returns to a configuration close to the initial horizontal alignment, leading to a corresponding recovery of the polarization characteristics of the emitted photon pairs.

Importantly, theoretical calculations demonstrate that the twisted molecular structure of FNLCs also enables a reconfigurable quasi-phase-matching mechanism. When the molecular twist period—whose optimal value is matched to the nonlinear coherence length of the SPDC process—the photon-pair generation efficiency scales quadratically with the sample length. Under these conditions, a 200 μm thick FNLC cell achieves a photon-pair rate approaching 1 MHz, which is ~625 times higher than that of a 7–8 μm thick sample. This effectively overcomes the long-standing bottleneck of low efficiency in tunable quantum light sources.

In summary, the generation of tunable entangled photon pairs based on FNLCs holds profound significance: it not only pioneers the introduction of LC materials into the field of quantum light sources, but also achieves the synergistic optimization of tunability, generation efficiency, and fabrication feasibility through the combination of electrical and geometric modulation, as well as high-efficiency quasi-phase matching technology. However, despite these breakthroughs, the research still has notable limitations: it has not yet realized complete photon entanglement, nor has it systematically explored the precise regulation of entanglement degree by sample geometric configurations and external fields.

To address these limitations, the research team further selected room-temperature FNLC-1751 (whose core component of the nonlinear polarizability tensor d_{33} is ~20 pm/V, with nonlinear response comparable to traditional nonlinear crystals) as the research object,[153] and designed various configurations of LC samples, including 180° twisted wedge cells (with thickness ranging from 2.5 to 20 μm), 5 μm thick 90° twisted cells, and 3.5 μm thick 180° twisted cells. A 450 nm continuous-wave laser was employed as the pump source, and combined with the Hanbury-Brown–Twiss interferometer and polarization tomography technology, the entanglement degree of photon pairs was quantified with concurrence as the core indicator, ultimately achieving controllable and reversible regulation of the polarization state and entanglement degree of photon pairs.[153]

Specifically, in the dimension of geometric modulation, the study found that the 180° twisted wedge cell can generate near-fully entangled photon pairs with a concurrence of 0.98 ± 0.06 at a thickness of 2.9 μm; with the increase in sample thickness, the entanglement degree decreases gradually, and the average purity of the generated

quantum states reaches as high as 0.92 ± 0.10. In the dimension of electrical field modulation, applying an electric field of 0–1.4 V/mm in the 90° twisted cell can increase the entanglement degree from 0.22 ± 0.05 to 0.94 ± 0.06; whereas an electric field of 1.25 V/mm in the 180° twisted cell can reduce the initial high entanglement degree of 0.89 ± 0.07 to 0.1 ± 0.1, and the electrical field modulation exhibits excellent reversibility. Moreover, sample flipping can further expand the coverage of achievable quantum states.

This groundbreaking progress not only realizes, for the first time, full-range entanglement degree regulation of photon pairs from fully separable to fully entangled in LC systems, but also verifies the feasibility of pixelated quantum light sources based on multi-electrode arrays. It provides a high-performance and customizable new quantum light source solution for quantum technologies such as quantum key distribution and quantum information processing, driving FNLC-based quantum optical devices to achieve a key leap from basic principle verification to engineering and practical application.

V. SUMMARY AND OUTLOOK

LCs, in particular, the emerging FNLCs developed in recent years, are experiencing a paradigmatic shift from conventional display media to multifunctional photonic platforms. This transition is manifested not only in the flexible and controllable regulation of linear electro-optical effects but also extends to the efficient modulation of nonlinear optical processes and innovative applications in quantum optics, thus fueling their rapid expansion in the fields of NLO and quantum photonics. Endowed with superior structural flexibility, linear electro-optical tunability, and high compatibility with diverse device configurations, LCs have achieved remarkable progress in multiple cutting-edge research directions. These include linear electro-optical modulation, SHG, nonlinear wavefront shaping, geometric phase manipulation based on spiral polarization textures, as well as the generation of entangled photons and the regulation of their polarization states. Nevertheless, the development of this promising material system is confronted with considerable challenges.

Despite their promising application prospects, the overall research on FNLCs remains in the preliminary stage, with a significant gap existing between proof-of-concept studies and large-scale practical implementations. Compared with traditional NLCs, FNLCs exhibit highly unconventional structural features and properties, which challenge the established understanding of nematic order in various aspects. Controversies persist concerning the microscopic origin of their polarity, detailed phase structures, and phase formation mechanisms, while the evolutionary pathway connecting the ferroelectric nematic phase and the ordinary nematic phase has not yet been fully elucidated. Multicomponent systems based on the ferroelectric nematic phase, such as polymer-stabilized FNLCs, polymer-dispersed FNLCs, and FNLC elastomers, are also anticipated to become prominent research directions in the future. Essentially, these FNLC-based multicomponent systems represent extensions centered on the core optical properties of FNLCs, and in-depth investigation of these properties is essential to clarify their inherent advantages and existing limitations. In summary, FNLCs integrate fundamental research value and practical application potential, rendering them a highly promising novel functional material system.

From the perspective of optical characteristics, the core advantage of FNLCs resides not only in the precise regulation of linear electro-optical responses but also in their distinctive nonlinear optical performance. This dual attribute, characterized by "flexible linear regulation and efficient nonlinear modulation," further lays a solid foundation for their applications in quantum optics. However, cautious consideration is still required when deploying these "liquid ferroelectrics" in ultrafast optoelectronic devices. Ultrafast electro-optical components are of crucial importance to modern communication technologies; yet, the performance of FNLC-based devices reported to date is not universally satisfactory, often demonstrating significant advantages only under specific device structures or operating conditions. According to existing research findings, the characteristic orientation time of FNLCs driven by in-plane electric fields typically remains in the millisecond range, and in-plane driving is not the most widely adopted electric field configuration in industrial applications. Under the more commonly used out-of-plane electric field, the performance becomes even less favorable: the response time frequently extends from hundreds of milliseconds to the second range, which is presumably associated with the relatively high viscosity of FNLCs. Additionally, out-of-plane electric fields tend to induce texture instability and reduce cycling reliability. When combined with additional challenges, such as high topological defect density and the difficulty in achieving stable near-vertical alignment, these factors collectively indicate that FNLCs at the current stage may not yet qualify as the ideal core material for truly ultrafast optoelectronic devices.

While challenges persist in the development of ultrafast optoelectronic devices based on FNLCs, their transformative potential in the field of nonlinear optics is driving a fundamental paradigmatic shift in this discipline: moving away from the traditional reliance on host-guest systems toward the utilization of intrinsic ferroelectric polar order. Although composite strategies incorporating nanoparticles and low-dimensional materials have successfully enhanced third-order nonlinear effects, the emergence of FNLCs offers a more revolutionary approach—they exhibit ultrahigh second-order polarizability $\chi^{(2)}$, comparable to that of inorganic solids. The focus of future research is likely to shift away from characterizing these fundamental coefficients toward designing stable and directly applicable device architectures. One key frontier direction involves stabilizing polar order through polymer networks: the transition from small-molecule systems to cross-linked polymers or elastomers is expected to address long-standing issues related to thermal stability and mechanical durability, thereby paving the way for the development of flexible and integrable nonlinear photonic devices.

The intersection of the nonlinear optical properties of FNLCs with topological photonics has sparked novel research opportunities, offering extensive exploration potential. The discovery of the helical ferroelectric phase, which possesses helical polar order and can significantly enhance SHG efficiency, suggests that soft matter systems may host complex optical topological protection mechanisms. This, in turn, holds promise for achieving stable and scatter-free frequency conversion and light transmission. Simultaneously, the concept of nonlinear geometric phase provides a new avenue for all-optical computing and information processing. By leveraging the intrinsic spin–orbit interaction inherent in nonlinear polarization processes, future devices are expected to realize dynamic and reconfigurable wavefront shaping as well as holographic projection, thus effectively integrating the fields of singular optics and nonlinear materials science.

The in-depth integration of such nonlinear properties and structural regulation further propels FNLCs from the realm of classical optics to the core of quantum optics research. LC-based systems are rapidly evolving from passive manipulation components to active

"engines" for quantum optical state generation, and FNLCs occupy a pivotal position in this transition due to their synergistic advantages in linear regulation and nonlinear performance. Historically, devices such as Q-plates have primarily served as converters for vortex beams and high-dimensional classical entanglement. However, the recent realization of the SPDC process in FNLC media marks the advent of a new era where soft matter emerges as a major source of entangled photons. The immediate focus of research in this field will be on expanding these isolated proof-of-concept experiments to integrated quantum circuit platforms. A unique advantage of FNLCs lies in their tunability, which enables the potential construction of "adaptive" quantum light sources—their entanglement properties, such as polarization state and spectral correlation, can be dynamically reconfigured to meet the requirements of dynamic quantum networks. Figure 14 systematically

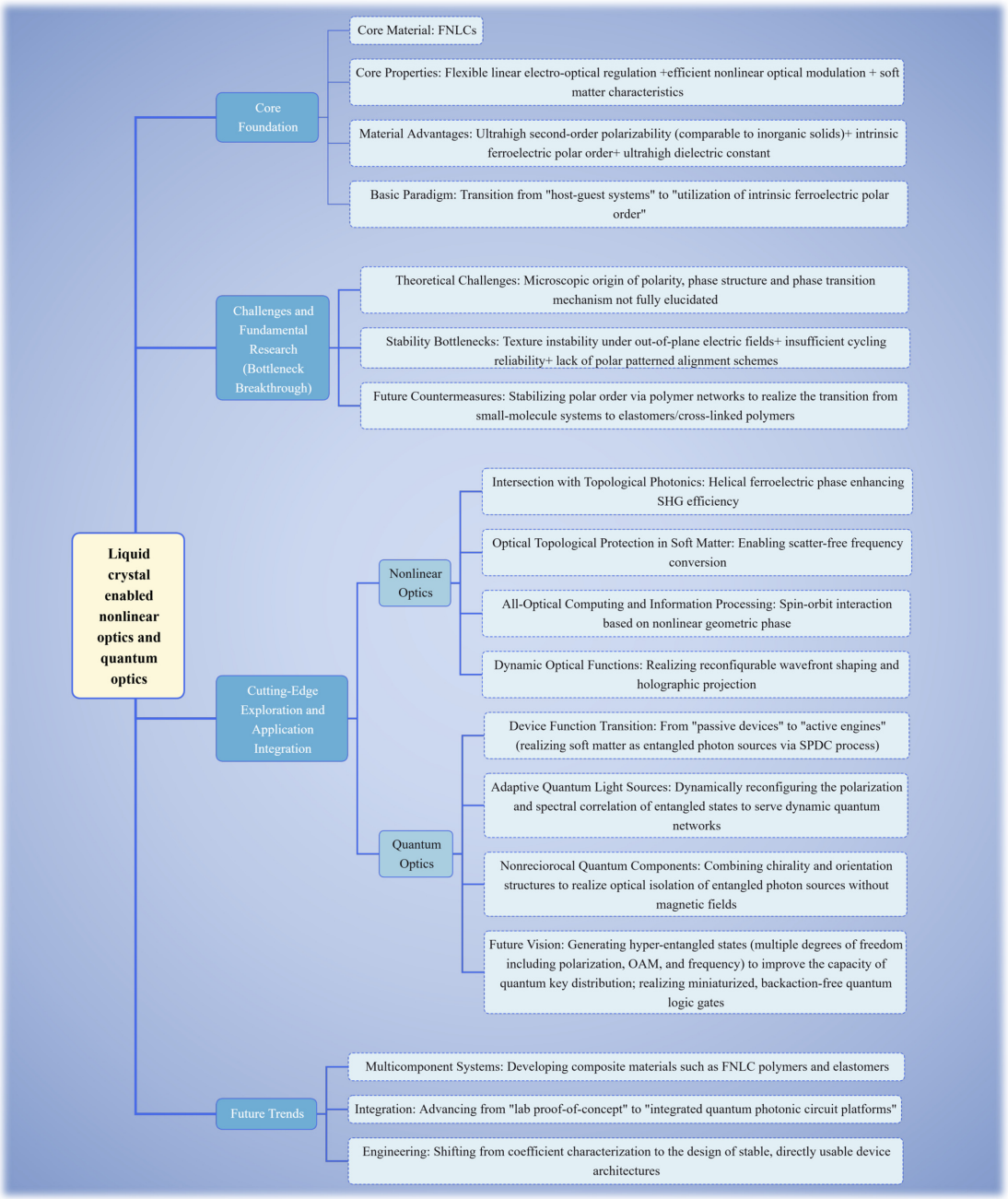

FIG. 14. Core framework and development outlook of FNLC-enabled nonlinear optics and quantum optics.

elaborates on FNLCs-enabled nonlinear optics and quantum optics, covering core foundations, fundamental research challenges and breakthroughs, cutting-edge exploration and application integration in nonlinear and quantum optics, as well as future trends in multicomponent systems, integration and engineering of this field.

The potential of such adaptive quantum light sources provides a new starting point for the innovation of quantum components. Specifically, the combination of chirality and orientation structures has opened up a novel paradigm for non-reciprocal quantum components. Research on the realization of directional entangled photon sources using helical structures has addressed a key bottleneck in quantum hardware: achieving optical isolation without the need for bulky magnetic field configurations. Looking forward, this platform is expected to be extended to the field of hyper-entanglement generation—by simultaneously regulating polarization, orbital angular momentum, and frequency degrees of freedom, the channel capacity of quantum key distribution can be significantly improved. Through the integration of the self-assembly precision of LCs with patterned alignment technologies, researchers may soon realize compact and backaction-free quantum logic gates and routers, which are critical for ensuring the scalability of future quantum internet architectures.

ACKNOWLEDGMENTS

This work was supported by the National Key Research and Development Program of China (2022YFA1405000 and 2025YFE0114700), the National Natural Science Foundation of China (Grant Nos. 62375119 and 62305033), the Natural Science Foundation of Jiangsu Province (BK20243067, BK20250164, and BK20232040), the Fundamental Research Funds for the Central Universities (Grant No. 2025300215), the Open Research Fund of State Key Laboratory of Quantum Functional Materials (QFM2025KF006), and the Chongqing Municipal Science and Technology Bureau (CSTB2025TIAD-KPX0063).

AUTHOR DECLARATIONS

Conflict of Interest

The authors have no conflicts to disclose.

Author Contributions

Li-Lan Tian, Fan Zou, and Jin-Tao Pan contributed equally to this paper.

Li-Lan Tian: Conceptualization (equal); Data curation (equal); Formal analysis (equal); Funding acquisition (equal); Investigation (equal); Methodology (equal). **Fan Zou:** Investigation (equal); Writing – original draft (equal); Writing – review & editing (equal). **Jin-Tao Pan:** Investigation (equal); Supervision (equal); Writing – review & editing (equal). **Ze-Nian Wu:** Investigation (equal); Resources (equal); Writing – review & editing (equal). **Yang Wei:** Investigation (equal); Writing – review & editing (equal). **Yi-Hao Wei:** Investigation (equal); Resources (equal); Supervision (equal); Writing – review & editing (equal). **Ling-Ling Ma:** Conceptualization (equal); Funding acquisition (equal); Investigation (equal); Resources (equal); Supervision (equal); Validation (equal); Visualization (equal); Writing – review & editing (equal). **Yan-Qing Lu:** Investigation (equal); Resources (equal); Supervision (equal); Writing – review & editing (equal).

DATA AVAILABILITY

The data that support the findings of this study are available from the corresponding author upon reasonable request. The data are not publicly available due to state restrictions such as privacy or ethical restrictions.

REFERENCES

[1]Z. Tang, C. Li, R. Pan, B. Wang, Y. Liu, Q. Wang, J. Tan, Y. Xiang, H. Yang, and J. Li, "$Ge_2Sb_2Se_4Te$-based optical switch with ultra-high contrast ratio by multilayer Fabry-Pérot cavity," Adv. Sci. **12**, 2412499 (2025).
[2]L.-L. Ma, S.-B. Wu, W. Hu, C. Liu, P. Chen, H. Qian, Y. Wang, L. Chi, and Y. Lu, "Self-assembled asymmetric microlenses for four-dimensional visual imaging," ACS Nano **13**, 13709–13715 (2019).
[3]L.-L. Ma, M. Tang, W. Hu, Z. Cui, S. Ge, P. Chen, L. Chen, H. Qian, L. Chi, and Y. Lu, "Smectic layer origami via preprogrammed photoalignment," Adv. Mater. **29**, 1606671 (2017).
[4]Z. Song, Z. Li, X. Shang, C. Li, L.-L. Ma, Y. Lu, and B. Li, "Electrically switchable structural patterns and diffractions in a dual frequency nematic liquid crystal," Chin. Opt. Lett. **21**, 010501 (2023).
[5]N. Wu, Y. Sun, J. Hu, C. Yang, Z. Bai, F. Wang, X. Cui, S. He, Y. Li, C. Zhang, K. Xu, J. Guan, S. Xiao, and Q. Song, "Intelligent nanophotonics: When machine learning sheds light," eLight **5**, 5 (2025).
[6]X. Yao, X. Hong, and Y. Liu, "Visible Mie resonances in dielectric hollow spheres: Principle, regulation, and applications," Responsive Mater. **1**, e20230019 (2023).
[7]X. Qiu, R. Zhang, Y. Ma, Z. Zhao, Z. Song, A. C. J. Orr, M. Li, W. Kamal, J. Guo, A. A. Castrejón-pita, S. J. Elston, S. M. Morris, and C. He, "Complex structured light generation using printed liquid crystal droplets," Adv. Opt. Mater. **13**, e02276 (2025).
[8]H. S. Yun, D. Wei, S. Yang, G. Park, M. S. Kim, T. J. Shin, D. M. Walba, M. J. Han, and D. K. Yoon, "Reconfigurable liquid crystal-based physical unclonable function integrating optical and electrical responses (Adv. Mater. 39/2025)," Adv. Mater. **37**, e70631 (2025).
[9]B. Kim, G. Park, G. Lee, J. Kim, C. Lee, J. G. Park, M. Kim, J. S. Myung, H. Ahn, S. M. Park, W. J. Choi, and D. K. Yoon, "Solvent-driven synthesis of DNA-based liquid crystalline organogels with extraordinary stretchability, self-healing, and higher-order structural assembly," Small **21**, 2500607 (2025).
[10]Y. Zhang, Z.-G. Zheng, and Q. Li, "Multiple degrees-of-freedom programmable soft-matter-photonics: Configuration, manipulation, and advanced applications," Responsive Mater. **2**, e20230029 (2024).
[11]Y. Xu, Y. Tang, and Q. Li, "Visible- and near-infrared light-driven molecular photoswitches for biological applications," Adv. Funct. Mater. **35**, 2416359 (2025).
[12]R. Zheng, Y. Wei, Z. C. Zhang, Z. Y. Wang, L. L. Ma, Y. Wang, L. Huang, and Y. Q. Lu, "Stimuli-responsive active materials for dynamic control of light field," Responsive Mater. **1**, e20230017 (2023).
[13]J. Chen, T. C. Xu, W. G. Zhao, L. L. Ma, D. Z. Chen, and Y. Q. Lu, "Photoresponsive thin films of well-synthesized azobenzene side-chain liquid crystalline polynorbornenes as command surface for patterned graphic writing," Polymer **218**, 123492 (2021).
[14]Z.-B. Fan, Y.-F. Cheng, Z.-M. Chen, X. Liu, W.-L. Lu, S.-H. Li, S.-J. Jiang, Z. Qin, and J.-W. Dong, "Integral imaging near-eye 3D display using a nanoimprint metalens array," eLight **4**, 3 (2024).
[15]J. Gao, Y. Tang, D. Martella, J. Guo, D. S. Wiersma, and Q. Li, "Stimuli-responsive photonic actuators for integrated biomimetic and intelligent systems," Responsive Mater. **1**, e20230008 (2023).
[16]P. Zhang, G. Wang, and H. Yu, "Ultraviolet-visible-near-infrared light-responsive soft materials: Fabrication, photomechanical deformation and applications," Responsive Mater. **2**, e20240016 (2024).
[17]L.-L. Ma, C.-Y. Li, J.-T. Pan, Y.-E. Ji, C. Jiang, R. Zheng, Z.-Y. Wang, Y. Wang, B.-X. Li, and Y.-Q. Lu, "Self-assembled liquid crystal architectures for soft matter photonics," Light: Sci. Appl. **11**, 270 (2022).
[18]L.-L. Ma, Y. Wei, N. Wang, W. Chen, and Y.-Q. Lu, "Soft matter photonics: Interplay of soft matter and light," ACS Nano **19**, 11501–11516 (2025).

[19]L.-Y. Sun, X.-Y. Wang, J.-H. Chen, C.-Y. Li, L.-L. Ma, Y.-Q. Lu, and B.-X. Li, "Electrical modification of order parameters and director fluctuations in a dielectrically negative nematic doped with a positive additive," J. Mol. Liq. **363**, 119843 (2022).
[20]L.-L. Ma, W. Duan, M.-J. Tang, L.-J. Chen, X. Liang, Y.-Q. Lu, and W. Hu, "Light-driven rotation and pitch tuning of self-organized cholesteric gratings formed in a semi-free film," Polymers **9**, 295 (2017).
[21]Y.-Y. Su, Z.-Q. Wang, H.-K. Jia, F. Chu, Q.-H. Wang, and T.-Z. Shen, "Frequency-dependent electro-optic properties of graphene oxide liquid crystal," Carbon **238**, 120199 (2025).
[22]L. Ma, C. Li, L. Sun, Z. Song, Y. Lu, and B. Li, "Submicrosecond electro-optical switching of one-dimensional soft photonic crystals," Photonics Res. **10**, 786 (2022).
[23]Z. Liu, Y. Zagzag, R. D. Kamien, and C. O. Osuji, "Director response of liquid crystals in spatially varying magnetic fields with antagonistic anchoring conditions," ACS Appl. Mater. Interfaces **16**, 70130–70137 (2024).
[24]Y. Xu, Y. Yao, W. Deng, J.-C. Fang, R. L. Dupont, M. Zhang, S. Copar, U. Tkalec, and X. Wang, "Magnetocontrollable droplet mobility on liquid crystal-infused porous surfaces," Nano Res. **16**, 5098–5107 (2023).
[25]H. Yang, C. Wang, G. Jin, and C. Yu, "Liquid crystal-embedded fiber optic Fabry Perot temperature sensor based on Vernier effect," Measurement **225**, 113910 (2024).
[26]M. Kiyoura, H. Kudo, K. Inoue, F. Ishiwari, T. Fukushima, N. Kurokawa, and M. Tokita, "Birefringence inversion in liquid crystalline poly(substituted methylene)s bearing side-on mesogens," J. Mater. Chem. C **13**, 4651–4657 (2025).
[27]R. Zheng, L. Ma, W. Feng, J. Pan, Z. Wang, Z. Chen, Y. Zhang, C. Li, P. Chen, H. K. Bisoyi, B. Li, Q. Li, and Y. Lu, "Autonomous self-sustained liquid crystal actuators enabling active photonic applications," Adv. Funct. Mater. **33**, 2301142 (2023).
[28]L.-L. Ma, C. Liu, S.-B. Wu, P. Chen, Q.-M. Chen, J.-X. Qian, S.-J. Ge, Y.-H. Wu, W. Hu, and Y.-Q. Lu, "Programmable self-propelling actuators enabled by a dynamic helical medium," Sci. Adv. **7**, eabh3505 (2021).
[29]W. Zhang, Z. Wu, L. Lin, Y. Liu, X. Tang, Y. Shen, and D. Luo, "Accurate and anti-interference control of computer vision-assisted light-driven liquid crystal elastomer actuator," Adv. Intell. Syst. **7**, 2400496 (2025).
[30]T. Ohzono, K. Katoh, C. Wang *et al.*, "Uncovering different states of topological defects in Schlieren textures of a nematic liquid crystal," Sci. Rep. **7**, 16814 (2017).
[31]B.-H. Liu, C.-L. Yuan, H.-L. Hu, H. Wang, Y.-W. Zhu, P.-Z. Sun, Z.-Y. Li, Z.-G. Zheng, and Q. Li, "Dynamically actuated soft heliconical architecture via frequency of electric fields," Nat. Commun. **13**, 2712 (2022).
[32]X. Chen, E. Korblova, D. Dong, X. Wei, R. Shao, L. Radzihovsky, M. A. Glaser, J. E. Maclennan, D. Bedrov, D. M. Walba, and N. A. Clark, "First-principles experimental demonstration of ferroelectricity in a thermotropic nematic liquid crystal: Polar domains and striking electro-optics," Proc. Natl. Acad. Sci. U. S. A. **117**, 14021–14031 (2020).
[33]D. M. Agra-Kooijman, H. Yoon, S. Dey, and S. Kumar, "Origin of weak layer contraction in De Vries smectic liquid crystals," Phys. Rev. E **89**, 032506 (2014).
[34]T.-H. Lin, D.-Y. Guo, C.-W. Chen, T.-M. Feng, W.-X. Zeng, P.-C. Chen, L.-Y. Wu, W.-M. Guo, L.-M. Chang, H.-C. Jau, C.-T. Wang, T. J. Bunning, and I. C. Khoo, "Directed crystalline symmetry transformation of blue-phase liquid crystals by reverse electrostriction," Nat. Commun. **15**, 7038 (2024).
[35]H.-F. Chen, X.-Y. Tao, J.-T. Pan, L.-L. Ma, C. Chen, W.-G. Zhu, W. Chen, and Y.-Q. Lu, "Recongurable nonlinear Pancharatnam-Berry diffractive optics with photopatterned ferroelectric nematics," Light: Sci. Appl. **14**, 314 (2025).
[36]J.-T. Pan, B.-H. Zhu, L.-L. Ma, W. Chen, G.-Y. Zhang, J. Tang, Y. Liu, Y. Wei, C. Zhang, Z.-H. Zhu, W.-G. Zhu, G. Li, Y.-Q. Lu, and N. A. Clark, "Nonlinear geometric phase coded ferroelectric nematic fluids for nonlinear soft-matter photonics," Nat. Commun. **15**, 8732 (2024).
[37]Z.-X. Li, Y.-P. Ruan, P. Chen, J. Tang, W. Hu, K.-Y. Xia, and Y.-Q. Lu, "Liquid crystal devices for vector vortex beams manipulation and quantum information applications [invited]," Chin. Opt. Lett. **19**, 112601 (2021).
[38]V. Sultanov, A. Kavčič, E. Kokkinakis, N. Sebastián, M. V. Chekhova, and M. Humar, "Tunable entangled photon-pair generation in a liquid crystal," Nature **631**, 294–299 (2024).
[39]M. Sharma, M. Tal, C. McDonnell, and T. Ellenbogen, "Electrically and all-optically switchable nonlocal nonlinear metasurfaces," Sci. Adv. **9**, eadh2353 (2023).
[40]V. Wang, V. Sheng, S. Liu, R. Zhao, T. Xu, T. Xu, F. Chen, and W. Krolikowski, "Wavelength-dependent nonlinear wavefront shaping in 3D nonlinear photonic crystal," Chin. Opt. Lett. **22**, 071901 (2024).
[41]D. Pile, "Quantum meets nanophotonics," Nat. Photonics **18**, 216–217 (2024).
[42]L. Tang, J. Tang, and K. Xia, "Chiral quantum optics and optical nonreciprocity based on susceptibility-momentum locking," Adv. Quantum Technol. **5**, 2200014 (2022).
[43]D. de Ceglia, A. Alù, D. N. Neshev, and C. De Angelis, "Analog image processing with nonlinear nonlocal flat optics," Opt. Mater. Express **14**, 92 (2024).
[44]M. Ren *et al.*, "Roadmap on nonlinear optics–focus on chinese research," JPhys Photonics **5**, 032501 (2023).
[45]S.-L. Li, Z.-Y. Chen, P. Chen, W. Hu, C. Huang, S.-S. Li, X. Hu, Y.-Q. Lu, and L.-J. Chen, "Geometric phase-encoded stimuli-responsive cholesteric liquid crystals for visualizing real-time remote monitoring: Humidity sensing as a proof of concept," Light: Sci. Appl. **13**, 27 (2024).
[46]C. Yang, C.-M. Guo, Y.-X. Wei, and H.-F. Zhang, "Electromagnetic detection design in liquid crystals Janus metastructures based on second harmonic generation," IEEE Trans. Instrum. Meas. **73**, 1 (2024).
[47]Z. Chen, H. Dong, Z. Chen, W. Choi, J.-X. Chen, K. O. Kenneth, and W. Hong, "380-GHz third harmonic signal generation using differentially pumped varactors in a CMOS voltage controlled oscillator," IEEE Trans. Circuits Syst. I: Regul. Pap. **72**, 3104 (2025).
[48]G. Thekkadath, M. Houde, D. England, P. Bustard, F. Bouchard, N. Quesada, and B. Sussman, "Gain-induced group delay in spontaneous parametric down-conversion," Phys. Rev. Lett. **133**, 203601 (2024).
[49]X. Shi, A. A. Baiju, V. Dhyani, S. Wang, S. S. Mohanraj, V. Leong, J. Sun, B. Deng, J. Zhang, Y. Wang, K. Rottwitt, H. Ou, and D. Zhu, "Spontaneous parametric down-conversion in 4H-SiC integrated platform," Laser Photonics Rev. **19**, 2500104 (2025).
[50]P. R. Sharapova, S. S. Kruk, and A. S. Solntsev, "Nonlinear dielectric nanoresonators and metasurfaces: Toward efficient generation of entangled photons," Laser Photonics Rev. **17**, 2200408 (2023).
[51]L. Zhang, Z. Li, D. Liu, C. Wu, H. Xu, and Z. Li, "Entangled x-ray photon pair generation by free-electron lasers," Phys. Rev. Lett. **131**, 073601 (2023).
[52]M. Valeri, P. Barigelli, B. Polacchi, G. Rodari, G. D. Santis, T. Giordani, G. Carvacho, N. Spagnolo, and F. Sciarrino, "Generation and characterization of polarization-entangled states using quantum dot single-photon sources," Quantum Sci. Technol. **9**, 025002 (2024).
[53]Y. Shen, E. C. Martínez, and C. Rosales-Guzmán, "Generation of optical skyrmions with tunable topological textures," ACS Photonics **9**, 296–303 (2022).
[54]J. Uchida, B. Soberats, M. Gupta, and T. Kato, "Advanced functional liquid crystals," Adv. Mater. **34**, 2109063 (2022).
[55]R. Friedrich, "Beiträge zur kenntniss des cholesterins," Monatsh. Chem. **9**, 421–441 (1888).
[56]I. Khoo, *Liquid Crystals*, 1st ed. (Wiley, 2022).
[57]I. Dierking, *Textures of Liquid Crystals*, 1st ed. (Wiley, 2003).
[58]D. Pauluth and K. Tarumi, "Optimization of liquid crystals for television," J. Soc. Inf. Disp. **13**, 693–702 (2005).
[59]A. Mertelj, L. Cmok, N. Sebastian, R. J. Mandle, R. R. Parker, A. C. Whitwood, J. W. Goodby, and M. Copic, "Splay nematic phase," Phys. Rev. X **8**, 041025 (2018).
[60]L. Lejcek, "Discontinuity walls and twist disclinations in smectic a liquid crystals," Mol. Cryst. Liq. Cryst. **330**, 259–266 (1999).
[61]P. Oswald, A. Dequidt, and G. Poy, "Lehmann effect in nematic and cholesteric liquid crystals: A review," Liq. Cryst. Rev. **7**, 142–166 (2019).
[62]R. B. Meyer, L. Liebert, L. Strzelecki, and P. Keller, "Ferroelectric liquid crystals," J. Phys., Lett. **36**, 69–71 (1975).
[63]H. Bock and W. Helfrich, "Two ferroelectric phases of a columnar dibenzopyrene," Liq. Cryst. **18**, 387–399 (1995).
[64]D. Vorländer, "Die richtung der kohlenstoff-valenzen in benzol-abkömmlingen," Ber. Dtsch. Chem. Ges. B **62**, 2831–2835 (1929).
[65]Y. Taguchi, C.-C. Yen, S. Kang, M. Tokita, and J. Watanabe, "Unusual transformation of the mechanically induced monodomain state to the polydomain one in polar nematic liquid crystals of aromatic polyesters," J. Phys. Chem. B **113**, 5341–5344 (2009).

[66]M. Koike, C.-C. Yen, L. Yuqing, H. Tsuchiya, M. Tokita, S. Kawauchi, H. Takezoe, and J. Watanabe, "Unusual nematic liquid crystal with polar cs symmetry formed from aromatic polyesters with head–tail character," Macromolecules **40**, 2524–2531 (2007).
[67]H. Takezoe, K. Kishikawa, and E. Gorecka, "Switchable columnar phases," J. Mater. Chem. **16**, 2412–2416 (2006).
[68]E. Gorecka, D. Pociecha, J. Mieczkowski, J. Matraszek, D. Guillon, and B. Donnio, "Axially polar columnar phase made of polycatenar bent-shaped molecules," J. Am. Chem. Soc. **126**, 15946–15947 (2004).
[69]K. Kishikawa, S. Nakahara, Y. Nishikawa, S. Kohmoto, and M. Yamamoto, "A ferroelectrically switchable columnar liquid crystal phase with achiral molecules: Superstructures and properties of liquid crystalline ureas," J. Am. Chem. Soc. **127**, 2565–2571 (2005).
[70]H. Takezoe, "Polar liquid crystals – ferro, antiferro, banana, and columnar," Mol. Cryst. Liq. Cryst. **646**, 46–65 (2017).
[71]R. B. Meyer, "Piezoelectric effects in liquid crystals," Phys. Rev. Lett. **22**, 918–921 (1969).
[72]M. Born, "Über anisotrope flüssigkeiten: Versuch einer theorie der flüssigen kristalle und des elektrischen kerr-effekts in flüssigkeiten," Sitzungsber. Preuss. Akad. Wiss. **30**, 614–650 (1916).
[73]R. J. Mandle, S. J. Cowling, and J. W. Goodby, "A nematic to nematic transformation exhibited by a rod-like liquid crystal," Phys. Chem. Chem. Phys. **19**, 11429–11435 (2017).
[74]H. Nishikawa, K. Shiroshita, H. Higuchi, Y. Okumura, Y. Haseba, S. Yamamoto, K. Sago, and H. Kikuchi, "A fluid liquid-crystal material with highly polar order," Adv. Mater. **29**, 1702354 (2017).
[75]F. C. Frank, "I. Liquid crystals. On the theory of liquid crystals," Discuss. Faraday Soc. **25**, 19–28 (1958).
[76]P. Palffy-Muhoray, M. A. Lee, and R. G. Petschek, "Ferroelectric nematic liquid crystals: Realizability and molecular constraints," Phys. Rev. Lett. **60**, 2303–2306 (1988).
[77]R. Berardi, M. Ricci, and C. Zannoni, "Ferroelectric nematic and smectic liquid crystals from tapered molecules," ChemPhysChem **2**, 443–447 (2001).
[78]R. Berardi, M. Ricci, and C. Zannoni, "Ferroelectric and structured phases from polar tapered mesogens," Ferroelectrics **309**, 3–13 (2004).
[79]R. J. Mandle, S. J. Cowling, and J. W. Goodby, "Rational design of rod-like liquid crystals exhibiting two nematic phases," Chem. - Eur. J. **23**, 14554–14562 (2017).
[80]A. Manabe, M. Bremer, and M. Kraska, "Ferroelectric nematic phase at and below room temperature," Liq. Cryst. **48**, 1079–1086 (2021).
[81]B. Huke and M. Lücke, "Magnetic properties of colloidal suspensions of interacting magnetic particles," Rep. Prog. Phys. **67**, 1731–1768 (2004).
[82]F. Bisi, A. M. Sonnet, and E. G. Virga, "Steric effects in a mean-field model for polar nematic liquid crystals," Phys. Rev. E **82**, 041709 (2010).
[83]A. Tudi, S. Han, Z. Yang, and S. Pan, "Potential optical functional crystals with large birefringence: Recent advances and future prospects," Coord. Chem. Rev. **459**, 214380 (2022).
[84]P. Weinberger, "John Kerr and his effects found in 1877 and 1878," Philos. Mag. Lett. **88**, 897–907 (2008).
[85]J. Valasek, "Properties of Rochelle salt related to the piezo-electric effect," Phys. Rev. **20**, 639–664 (1922).
[86]P. A. Franken and J. F. Ward, "Optical harmonics and nonlinear phenomena," Rev. Mod. Phys. **35**, 23–39 (1963).
[87]J. A. Armstrong, N. Bloembergen, J. Ducuing, and P. S. Pershan, "Interactions between light waves in a nonlinear dielectric," Phys. Rev. **127**, 1918–1939 (1962).
[88]P. M. Rentzepis and Y. H. Pao, "Laser-induced optical second harmonic generation in organic crystals," Appl. Phys. Lett. **5**, 156–158 (1964).
[89]B. L. Davydov, L. D. Derkacheva, V. V. Dunina, M. E. Zhabotinskii, and M. A. Samokhina, "Connection between charge transfer and laser second harmonic generation," J. Exp. Theor. Phys. Lett. **12**, 16 (1970).
[90]A. N. Gowda, M. Kumar, A. R. Thomas *et al.*, "Self-assembly of silver and gold nanoparticles in a metal-free phthalocyanine liquid crystalline matrix: Structural, thermal, electrical and nonlinear optical characterization," ChemistrySelect **1**, 1361–1370 (2016).
[91]H. C. Lin, A. Y. G. Fuh, C. Y. Lin *et al.*, "Enhancement of optical nonlinearity of LCs with gold-nanoparticle-doped alignment layers," Proc. SPIE **8772**, 87721G (2013).
[92]H. Mbarak, A. K. Kodeary, S. M. Hamidi *et al.*, "Control of nonlinear refractive index of AuNPs doped with nematic liquid crystal under external electric field," Optik **198**, 163299 (2019).
[93]T. Vimal, K. Agrahari, R. K. Sonker *et al.*, "Investigation of thermodynamical, dielectric and electro-optical parameters of nematic liquid crystal doped with polyaniline and silver nanoparticles," J. Mol. Liq. **290**, 111241 (2019).
[94]Z. Dehghani, N. Dalir, M. Nadafan *et al.*, "Investigation of electrical and nonlinear optical properties of colloidal composite nematic liquid crystal," J. Mol. Liq. **225**, 502–509 (2017).
[95]K. P. Praseetha, M. C. Divyasree, K. Chandrasekharan *et al.*, "Enhanced optical nonlinearity in nematic liquid crystal on doping with CdSe quantum dot," J. Mol. Liq. **273**, 497–503 (2019).
[96]K. P. Praseetha, E. Shiju, K. Chandrasekharan *et al.*, "Intense nonlinear optical properties of ZnS quantum dot doped nematic liquid crystal compounds," J. Mol. Liq. **328**, 115347 (2021).
[97]S. Li, M. Fu, H. Sun *et al.*, "Enhanced photorefractive and third-order nonlinear optical properties of 5CB-based polymer-dispersed liquid crystals by graphene doping," J. Phys. Chem. C **118**, 18015–18020 (2014).
[98]S. Naserbakht, A. Maleki, S. Mohajer *et al.*, "Nonlinear optical response of liquid crystalline matrix doped with single walled carbon nanotube and graphene sheets," J. Mol. Liq. **222**, 1212–1217 (2016).
[99]B. Mhmaa and C. Zd, "Improvement of the third order nonlinear optical properties of nematic liquid crystal under the influence of different compositional percentage of doped SWCNT and the external electric field," J. Mol. Liq. **275**, 281–289 (2019).
[100]P. Kumar, V. Sharma, C. Jaggi, P. Malik, and K. K. Raina, "Orientational control of liquid crystal molecules via carbon nanotubes and dichroic dye in polymer dispersed liquid crystal," Liq. Cryst. **44**, 843–853 (2017).
[101]K. P. Praseetha, K. Chandrasekharan, and S. Varghese, "Optical behaviour of nematic liquid crystal doped with carbon dot in the nonlinear optical regime," Opt. Laser Technol. **130**, 106367 (2020).
[102]G. S. He, T. C. Lin, P. N. Prasad *et al.*, "Optical power limiting and stabilization using a two-photon absorbing neat liquid crystal in isotropic phase," Appl. Phys. Lett. **82**, 4717–4719 (2003).
[103]V. A. Enikeeva, A. Zolot'Ko, V. A. Makarov *et al.*, "Second harmonic generation by femtosecond pulses in nematic liquid crystal," Bull. Lebedev Phys. Inst. **34**, 142–145 (2007).
[104]N. Murazawa, S. Juodkazis, H. Misawa *et al.*, "Two-photon excitation of dye-doped liquid crystal by a CW-laser irradiation," Mol. Cryst. Liq. Cryst. **489**, 310–319 (2008).
[105]X. Wen, T. Liu, J. Fan, K. Gong, and J. Song, "Electrically controlled liquid crystal nonlinear optical devices prepared by multi-layer composite structures," J. Mol. Liq. **382**, 121889 (2023).
[106]J. Li, H. Nishikawa, J. Kougo, J. Zhou, S. Dai, W. Tang, X. Zhao, Y. Hisai, M. Huang, and S. Aya, "Development of ferroelectric nematic fluids with giant-ε dielectricity and nonlinear optical properties," Sci. Adv. **7**, eabf5047 (2021).
[107]X. Zhao, J. Zhou, J. Li, J. Kougo, Z. Wan, M. Huang, and S. Aya, "Spontaneous helielectric nematic liquid crystals: Electric analog to helimagnets," Proc. Natl. Acad. Sci. U. S. A. **118**, e2111101118 (2021).
[108]T. D. Huang and T. H. Lu, "Controlling an optical vortex array from a vortex phase plate, mode converter, and spatial light modulator," Opt. Lett. **44**, 3917 (2019).
[109]A. Komar, Z. Fang, J. Bohn, J. Sautter, M. Decker, A. Miroshnichenko, T. Pertsch, I. Brener, Y. S. Kivshar, I. Staude, and D. N. Neshev, "Electrically tunable all-dielectric optical metasurfaces based on liquid crystals," Appl. Phys. Lett. **110**, 071109 (2017).
[110]D. Wang, F. Liu, T. Liu, Q. Sun, Q. He, and L. Zhou, "Efficient generation of complex vectorial optical fields with metasurfaces," Light: Sci. Appl. **10**, 67 (2021).
[111]Y. Chen, K.-Y. Xia, W.-G. Shen, J. Gao, Z.-Q. Yan, Z.-Q. Jiao, J.-P. Dou, H. Tang, Y.-Q. Lu, and X.-M. Jin, "Vector vortex beam emitter embedded in a photonic chip," Phys. Rev. Lett. **124**, 153601 (2020).
[112]X. Yi, Y. Liu, X. Ling, X. Zhou, Y. Ke, H. Luo, S. Wen, and D. Fan, "Hybrid-order poincaré sphere," Phys. Rev. A **91**, 023801 (2015).
[113]G. Milione, D. A. Evans, D. R. Nolan, and R. R. Alfano, "Higher order Pancharatnam-Berry phase and the angular momentum of light," Phys. Rev. Lett. **108**, 190401 (2012).

[114]G. Milione, H. S. Izzat, D. A. Nolan, and R. R. Alfano, "Higher-order poincaré sphere, stokes parameters, and the angular momentum of light," Phys. Rev. Lett. **107**, 053601 (2011).
[115]B. Ndagano, R. Brüning, M. McLaren, M. Duparré, and A. Forbes, "Fiber propagation of vector modes," Opt. Express **23**, 17330 (2015).
[116]W. Qiao, T. Lei, Z. Wu, S. Gao, Z. Li, and X. Yuan, "Approach to multiplexing fiber communication with cylindrical vector beams," Opt. Lett. **42**, 2579 (2017).
[117]G. Milione, M. P. J. Lavery, H. Huang, Y. Ren, G. Xie, T. A. Nguyen, E. Karimi, L. Marrucci, D. A. Nolan, R. R. Alfano, and A. E. Willner, "4 × 20 Gbit/s mode division multiplexing over free space using vector modes and a q-plate mode (de)multiplexer," Opt. Lett. **40**, 1980 (2015).
[118]M. McLaren, T. Konrad, and A. Forbes, "Measuring the nonseparability of vector vortex beams," Phys. Rev. A **92**, 023833 (2015).
[119]B. Ndagano, I. Nape, M. A. Cox, C. Rosales-Guzman, and A. Forbes, "Creation and detection of vector vortex modes for classical and quantum communication," J. Lightwave Technol. **36**, 292 (2018).
[120]C. Rosales-Guzman, B. Ndagano, and A. Forbes, "A review of complex vector light fields and their applications," J. Opt. **20**, 123001 (2018).
[121]P. Yue, D. Jianping, and W. Hutian, "Manipulation on novel vector optical fields: Introduction, advances and applications," Acta Opt. Sin. **39**, 0126001 (2019).
[122]A. Rubano, F. Cardano, B. Piccirillo, and L. Marrucci, "Q-plate technology: A progress review [invited]," J. Opt. Soc. Am. B **36**, D70 (2019).
[123]L. Marrucci, C. Manzo, and D. Paparo, "Optical spin-to-orbital angular momentum conversion in inhomogeneous anisotropic media," Phys. Rev. Lett. **96**, 163905 (2006).
[124]W. Ji, C.-H. Lee, P. Chen, W. Hu, Y. Ming, L. Zhang, T.-H. Lin, V. Chigrinov, and Y.-Q. Lu, "Meta-q-plate for complex beam shaping," Sci. Rep. **6**, 25528 (2016).
[125]L. Marrucci, E. Karimi, S. Slussarenko, B. Piccirillo, E. Santamato, E. Nagali, and F. Sciarrino, "Spin-to-orbital conversion of the angular momentum of light and its classical and quantum applications," J. Opt. **13**, 064001 (2011).
[126]E. Cohen, H. Larocque, F. Bouchard, F. Nejad sattari, Y. Gefen, and E. Karimi, "Geometric phase from aharonov-bohm to Pancharatnam-Berry and beyond," Nat. Rev. Phys. **1**, 437 (2019).
[127]L. Marrucci, E. Nagali, F. Sciarrino, L. Sansoni, F. De Martini, B. Piccirillo, E. Karimi, and E. Santamato, "Photonic quantum information applications of patterned liquid crystals," Mol. Cryst. Liq. Cryst. **526**, 108 (2010).
[128]A. Lohrmann, C. Perumgatt, and A. Ling, "Manipulation and measurement of quantum states with liquid crystal devices," Opt. Express **27**, 13765 (2019).
[129]E. Nagali, F. Sciarrino, F. De Martini, L. Marrucci, B. Piccirillo, E. Karimi, and E. Santamato, "Quantum information transfer from spin to orbital angular momentum of photons," Phys. Rev. Lett. **103**, 013601 (2009).
[130]B. Ndagano, B. Perez-Garcia, F. S. Roux, M. McLaren, C. Rosales-Guzman, Y. Zhang, O. Mouane, R. I. Hernandez-Aranda, T. Konrad, and A. Forbes, "Characterizing quantum channels with non-separable states of classical light," Nat. Phys. **13**, 397 (2017).
[131]V. Parigi, V. D'Ambrosio, C. Arnold, L. Marrucci, F. Sciarrino, and J. Laurat, "Storage and retrieval of vector beams of light in a multiple-degree-of-freedom quantum memory," Nat. Commun. **6**, 7706 (2015).
[132]X. Li, X. Liu, Z.-Q. Zhou, C.-F. Li, and G.-C. Guo, "Solid-state quantum memory for hybrid entanglement involving three degrees of freedom," Phys. Rev. A **101**, 052330 (2020).
[133]V. D'Ambrosio, G. Carvacho, F. Graffitti, C. Vitelli, B. Piccirillo, L. Marrucci, and F. Sciarrino, "Entangled vector vortex beams," Phys. Rev. A **94**, 030304 (2016).
[134]A. Sit, F. Bouchard, R. Fickler, J. Gagnon-Bischoff, H. Larocque, D. Heshami, C. Elser, K. Peuntinger, K. Günthner, B. Heim, C. Marquardt, G. Leuchs, R. W. Boyd, and E. Karimi, "High-dimensional intracity quantum cryptography with structured photons," Optica **4**, 1006 (2017).
[135]F. Graffitti, V. D'Ambrosio, M. Proietti, J. Ho, B. Piccirillo, C. de Lisio, L. Marrucci, and A. Fedrizzi, "Hyperentanglement in structured quantum light," Phys. Rev. Res. **2**, 043350 (2020).
[136]C. Rosales-Guzman, N. Bhebe, N. Mahonisi, and A. Forbes, "Multiplexing 200 spatial modes with a single hologram," J. Opt. **19**, 113501 (2017).
[137]E. Otte, K. Tekce, and C. Denz, "Spatial multiplexing for tailored fully-structured light," J. Opt. **20**, 105606 (2018).
[138]A. Trichili, C. Rosales-Guzmán, A. Dudley, B. Ndagano, A. Ben Salem, M. Zghal, and A. Forbes, "Optical communication beyond orbital angular momentum," Sci. Rep. **6**, 27674 (2016).
[139]E. Otte, C. Rosales-Guzmán, B. Ndagano, C. Denz, and A. Forbes, "Entanglement beating in free space through spin-orbit coupling," Light: Sci. Appl. **7**, 18009 (2018).
[140]Y.-H. Zhang, S.-J. Liu, P. Chen, D. Zhu, W. Chen, S.-J. Ge, Y. Wang, Z.-F. Zhang, and Y.-Q. Lu, "Logical rotation of non-separable states via uniformly self-assembled chiral superstructures," Nat. Commun. **15**, 1108 (2024).
[141]F. Cardano, M. Maffei, F. Massa, B. Piccirillo, C. de Lisio, G. De Filippis, V. Catudella, E. Santamato, and L. Marrucci, "Statistical moments of quantum-walk dynamics reveal topological quantum transitions," Nat. Commun. **7**, 11439 (2016).
[142]A. D'Errico, F. Cardano, M. Maffei, A. Dauphin, R. Barboza, C. Esposito, B. Piccirillo, M. Lewenstein, P. Massignan, and L. Marrucci, "Two-dimensional topological quantum walks in the momentum space of structured light," Optica **7**, 108 (2020).
[143]D. Cozzolino, B. Da Lio, D. Bacco, and L. K. Oxenlowe, "High-dimensional quantum communication: Benefits, progress, and future challenges," Adv. Quantum Technol. **2**, 1900038 (2019).
[144]A. Gratsea, F. Metz, and T. Busch, "Universal and optimal coin sequences for high entanglement generation in 1D discrete time quantum walks," J. Phys. A: Math. Theor. **53**, 445306 (2020).
[145]T. Giordani, E. Polino, S. Emiliani, A. Suprano, L. Innocenti, H. Majury, L. Marrucci, M. Paternostro, A. Ferraro, N. Spagnolo, and F. Sciarrino, "Experimental engineering of arbitrary qudit states with discrete-time quantum walks," Phys. Rev. Lett. **122**, 020503 (2019).
[146]T. Giordani, L. Innocenti, A. Suprano, E. Polino, M. Paternostro, N. Spagnolo, F. Sciarrino, and A. Ferraro, "Entanglement transfer, accumulation and retrieval via quantum-walk-based qubit-qudit dynamics," New J. Phys. **23**, 023012 (2021).
[147]T. Giordani, A. Suprano, E. Polino, F. Acanfora, L. Innocenti, A. Ferraro, M. Paternostro, N. Spagnolo, and F. Sciarrino, "Machine learning-based classification of vector vortex beams," Phys. Rev. Lett. **124**, 160401 (2020).
[148]F. Bouchard, A. Sit, Y. Zhang, R. Fickler, F. M. Miato, Y. Yao, F. Sciarrino, and E. Karimi, "Two-photon interference: The Hong-Ou-Mandel effect," Rep. Prog. Phys. **84**, 012402 (2021).
[149]E. Nagali, L. Sansoni, F. Sciarrino, F. De Martini, L. Marrucci, B. Piccirillo, E. Karimi, and E. Santamato, "Optimal quantum cloning of orbital angular momentum photon qubits through Hong-Ou-Mandel coalescence," Nat. Photonics **3**, 720 (2009).
[150]V. D'Ambrosio, G. Carvacho, I. Agresti, L. Marrucci, and F. Sciarrino, "Tunable two-photon quantum interference of structured light," Phys. Rev. Lett. **122**, 013601 (2019).
[151]M. Hiekkamäki and R. Fickler, "High-dimensional two-photon interference effects in spatial modes," Phys. Rev. Lett. **126**, 123601 (2021).
[152]M. Koni, F. Nothlawala, V. Hakobyan, I. Nape, E. Brasselet, and A. Forbes, "Dual-wavelength quantum skyrmions from liquid crystal topological defect," arXiv:2507.22815 (2025).
[153]S. Klopčič, A. Kavčič, N. Sebastián, and M. Humar, "Electrically and geometrically tunable photon pair entanglement from ferroelectric nematic liquid crystal," Adv. Sci. **13**, e15206 (2026).